In vitro and in vivo toxicity of thiolated and PEGylated organosilica nanoparticles

International Journal of Pharmaceutics 652 (2024) 123852

Contents lists available at ScienceDirect

International Journal of Pharmaceutics

journal homepage: www.elsevier.com/locate/ijpharm

In vitro and *in vivo* toxicity of thiolated and PEGylated organosilica nanoparticles

Balnur A. Zhaisanbayeva [a,b], Ellina A. Mun [b,*], Leila Ulmanova [b], Zarina Zhunissova [b], Bauyrzhan Umbayev [c], Farkhad Olzhayev [c], Ivan A. Vorobjev [b,c], Gonzalo Hortelano [b], Vitaliy V. Khutoryanskiy [d,*]

[a] School of Engineering and Digital Science, Nazarbayev University, 010000 Astana, Kazakhstan
[b] School of Sciences and Humanities, Nazarbayev University, 010000 Astana, Kazakhstan
[c] National Laboratory Astana, Nazarbayev University, 010000 Astana, Kazakhstan
[d] School of Pharmacy, University of Reading, Reading, UK

ARTICLE INFO

Keywords:
Thiolated organosilica nanoparticles
PEGylation
Biocompatibility
Cytotoxicity

ABSTRACT

This study comprises the comprehensive toxicological assessment of thiolated organosilica nanoparticles (NPs) synthesised from 3-mercaptopropyltrimethoxysilane (MPTS). We investigated the influence of three different types of nanoparticles synthesised from 3-mercaptopropyltrimethoxysilane: the starting thiolated silica (Si-NP-SH) and their derivatives prepared by surface PEGylation with PEG 750 (Si-NP-PEG750) and 5000 Da (Si-NP-PEG5000) on biological subjects from *in vitro* to *in vivo* experiments to explore the possible applications of those nanoparticles in biomedical research.

As a result of this study, we generated a comprehensive understanding of the toxicological properties of these nanoparticles, including their cytotoxicity in different cell lines, hemolytic properties, *in vitro* localisation, mucosal irritation properties and biodistribution in BALB/c mice. Our findings indicate that all three types of nanoparticles can be considered safe and have promising prospects for use in biomedical applications. Nanoparticles did not affect the viability of HPF, MCF7, HEK293 and A549 cell lines at low concentrations (up to 100 μg/mL); moreover, they did not cause organ damage to BALB/c mice at concentrations of 10 mg/kg.

The outcomes of this study enhance our understanding of the impact of organosilica nanoparticles on health and the environment, which is vital for developing silica nanoparticle-based drug delivery systems and provides opportunities to expand the applications of organosilica nanoparticles.

1. Introduction

In recent years, nanoparticles have gained much interest for their applications in the pharmaceutical and biomedical sciences. Expected outcomes of such applications include both *in vitro* and *in vivo* diagnostics, the production of improved biocompatible materials and drug delivery systems.

The significant advantages of nanoparticles include their small size that can be controlled during the synthesis, high surface area to volume ratio, biocompatibility, simplicity in production and easy surface modifications(Kumar, 2010). Among inorganic nanoparticles, silica or silica-coated materials are promising candidates for biomedical applications due to their small size, chemical and colloidal stability, and higher surface reactivity(Park et al., 2016; Murugadoss et al., 2017). These properties open numerous applications of silica nanoparticles in industry, material science, food, cosmetics, drug delivery, imaging technologies and tissue engineering(Wang et al., 2020). The presence of silanol groups on the surface of these nanoparticles provides an additional advantage of surface modification, thus directing biological properties and enabling toxicity reduction(Ahmadi et al., 2022; Chen et al., 2022).

Inorganic silica nanoparticles with silanol groups on their surface may form weak hydrogen bonds with some drug molecules. As these bonds are weak, it is insufficient for controlled drug release; therefore,

* Corresponding authors.
E-mail addresses: balnur.zhaisanbayeva@nu.edu.kz (B.A. Zhaisanbayeva), ellina.mun@nu.edu.kz (E.A. Mun), leila.ulmanova@alumni.nu.edu.kz (L. Ulmanova), zarina.zhunissova@alumni.nu.edu.kz (Z. Zhunissova), bauyrzhan.umbayev@nu.edu.kz (B. Umbayev), folzhayev@nu.edu.kz (F. Olzhayev), ivan.vorobyev@nu.edu.kz (I.A. Vorobjev), gonzalo.hortelano@nu.edu.kz (G. Hortelano), v.khutoryanskiy@reading.ac.uk (V.V. Khutoryanskiy).

https://doi.org/10.1016/j.ijpharm.2024.123852
Received 19 July 2023; Received in revised form 22 January 2024; Accepted 23 January 2024
Available online 26 January 2024

more studies are focusing on developing silica nanoparticles with organic components in their structure(Xiong and Qiao, 2016; Yu et al., 2018). An immense number of researchers use two-step synthesis to prepare organosilica nanoparticles, which uses TEOS as a core with the addition of organosilanes during or after the synthesis to incorporate organic groups (Sponchia et al., 2014; Roy et al., 2005; Cheng et al., 2019; Tsai et al., 2019; Sponchia et al., 2014). This method is also used to functionalise the outer surface of the nanoparticles for further modification with ligands or drugs. Intriguingly, organosilanes are rarely used as a single source of silica nanoparticles; however, there is a possibility for their production using a simple one-pot synthesis, and functional groups of organic nature could be incorporated into their structure. The synthesis of thiolated silica nanoparticles was previously reported using thiol-containing organosilanes such as 3-mercaptopropyltrimethoxysilane (MPTS) by Nakamura et al. (Nakamura and Ishimura, 2007) and Irmukhametova et al. (Irmukhametova et al., 2011). Furthermore, by varying the thiol-organosilane, 3-mercaptopropylethoxisilane (MPES), 3-mercaptopropylmethyldimethoxysilane (MPDMS), solvents and catalysts, the size, shape and charge of nanoparticles can be controlled(Nakamura et al., 2011; Nakamura and Ishimura, 2008; Al Mahrooqi et al., 2018). These nanoparticles are distinguished by the presence of thiol groups on the surface and in the bulk, allowing further functionalisation via reactions with various molecules.

Recent findings suggest that coating magnetic nanoparticles (Fe_3O_4, ZnO) with silica shells increases their biocompatibility by reducing cytotoxicity and improving their degradation and clearance(Navarro-Palomares et al., 2020). Other studies reported that the cytotoxicity and genotoxicity of silica nanoparticles were highly dependent on their type, size, dose and cell line used(Ding et al., 2018; Zhou et al., 2019; Mohammadpour et al., 2019; Decan et al., 2016). Nevertheless, more and more studies suggest that larger nanoparticles (>100 nm) disrupt the cell membrane and cause ruptures, while smaller nanoparticles (<100 nm) cause no damage upon penetration through the cell membrane(Park et al., 2016; Mohammadpour et al., 2019). However, small nanoparticles capable of getting incorporated between DNA gaps may induce genotoxicity through DNA strand breaks(Maser et al., 2015; Krętowski et al., 2017) and the optimal size of nanoparticles to safely internalise is around sub-100 nm(Dolai et al., 2021; Yim et al., 2017; Villanueva-Flores et al., 2020).

Another critical factor affecting nanoparticle properties is their surface and charge. The charge of nanoparticles affects the internalisation as well as the fate inside the cells. Some studies suggest that the positively charged nanoparticles have higher cellular uptake but might induce cell membrane disruptions. Positively charged nanoparticles may also induce thrombosis *in vivo*(Villanueva-Flores et al., 2020; Soddu et al., 2020).

When designing nanoparticles, it is also important to consider the behavior of NPs *in vivo*. This means that nanoparticles should maintain their colloidal stability to avoid activation of mononuclear phagocyte system (MPS), not form agglomerates, and not stimulate bleeding or/and thrombosis *in vivo*. Thus, their polydispersity, surface parameters and charge should be carefully controlled to allow longer circulation time, safety to blood vessels and blood itself, as well as having a route of excretion(Patsula et al., 2019). Many publications report that the functionalisation of inorganic nanoparticles with various polymers enhances the protection from the MPS, improves their dispersity, thus decreasing toxicity, and increases the tropism towards cancer cells (Nafee et al., 2007; Kulkarni and Feng, 2011; Shahabi et al., 2015; Kurtz-Chalot et al., 2017).

The most common polymers for these purposes include chitosan, polyethyleneimine (PEI) and polyethylene glycol (PEG), which are FDA-approved and are currently used in drug and gene delivery systems. A recent study by Li et al (Li et al., 2020), comparing chitosan, PEI and PEG-coated gold nanoparticles, demonstrated that the circulation time of PEGylated nanoparticles was several-fold longer compared to the NPs with a coating made of chitosan and PEI. Additionally, chitosan and PEI-coated nanoparticles tend to build up in the liver, which induces hepatic damage and provokes an immunological reaction by down-regulating cytochrome P450-related genes that induce inflammation(Li et al., 2020; Schuck et al., 2014). Various studies suggest that PEGylation of nanoparticles augments biostability, decreases toxicity, and escapes from the macrophage system, thus avoiding immune response and providing higher efficiency of cytotoxic agents through extended circulation time(Patsula et al., 2019; Ghaferi et al., 2020; Emam et al., 2019; Domac et al., 2020; Fiandra et al., 2020).

After confirming the effectiveness of the nanoparticle-based formulations, the next major concern that nanotechnology in pharmaceutical sciences has recently been facing is the fate of nanoparticles at the application site and their interaction within living systems(Wozniak et al., 2006; Wang et al., December 2022; Mishra et al., December 2022). Usually, every study on nanoparticle-based technology provides an *in vitro* evaluation of the developed formulation using MTT analysis, which is the golden standard for assessing cell viability, proliferation or cytotoxicity upon the effect of nanoparticles(Eswari et al., 2022; Amin et al., 2023; Al-shuwaili et al., 2023; Ilbasmis-Tamer et al., 2023). Other studies concerning *in vivo* analysis usually provide histology tests of the biological tissues of interest(Kashif et al., 2022). Formulations designed for systemic applications are studied for hemolytic compatibility with the patient's blood(Yan et al., 2022; Zhou et al., 2022). However, very rarely a comprehensive analysis of toxicity and biocompatibility of the developed system is provided. To the best of our knowledge, no such studies exist concerning MPTS-based organosilica nanoparticles, whilst their potential use as drug delivery vehicles and bioimaging agents has been investigated for the last few decades. Applying a systematic approach in studying the toxicity and biocompatibility of nanoparticles is extremely important, as there is no guarantee that the nanoparticle-based formulation will be exposed to the targeted site only and that the effect on the other tissues, organs and systems will be eliminated.

In this study, we assessed the toxicity of organosilica nanoparticles synthesised from (3-mercaptopropyl)tri-methoxysilane through its hydrolysis and self-condensation, which ultimately can be used as a drug carrier or a diagnostics tool. The size of nanoparticles can be controlled during the synthesis, and the optimal size of 45–50 nm was reported previously(Irmukhametova et al., 2011). We examined the interactions between organosilica nanoparticles and biological systems such as cells and tissues to determine how these interactions can be controlled or modulated for specific biomedical applications. Nanoparticles conjugated with PEG of various molecular weights were evaluated to achieve the most suitable NP design for future applications. In this study, we generated toxicological profiles of thiolated (Si NP-SH), PEGylated with PEG of 750 Da (Si NP-PEG750) and 5000 Da (Si NP-PEG5000) organosilica nanoparticles *in vitro* and *in vivo*. We believe that the outcomes of this research will significantly contribute to the existing knowledge about the effects of organosilica nanoparticles on biological systems. To the best of our knowledge this is the first study reporting a comprehensive toxicological evaluation of thiolated organosilica nanoparticles both *in vitro* and *in vivo*.

2. Materials and methods

2.1. Materials

(3-Mercaptopropyl)trimethoxysilane (MPTS, 95%), methoxy polyethylene glycol maleimide with molecular weights 750 Da (PEG750) and 5000 Da (PEG5000), Atto 488 maleimide, dimethyl sulfoxide (DMSO), 5,5′- dithiobis(2-nitrobenzoic acid) (DTNB), sodium hydroxide, L-cysteine hydrochloride, dimethylformamide (DMF), Dulbecco's modified eagle medium (DMEM), fetal bovine serum (FBS) and hematoxylin were purchased from Sigma Aldrich. Alexa 555 Phalloidin, Triton X-100, DAPI, and Alexa Fluor 750 C5 maleimide were purchased from Thermo Fisher, USA. CellTiter Cell proliferation assay was

purchased from Promega, USA.

2.2. Synthesis of thiolated and PEGylated organosilica nanoparticles

The synthesis of thiolated silica nanoparticles was performed according to the protocol of Mun et al. (Mun et al., 2014). Briefly, 1.125 mL of MPTS was added to 30 mL DMSO and 0.750 mL 0.5 M NaOH and stirred at room temperature for 24 h with air bubbling. After the completion of the reaction, nanoparticles were purified by dialysis against deionized water with dialysis tubes of 12000–14000 Da molecular weight cut-off for eight water changes. Further, a portion of thiolated nanoparticles was taken for PEGylation. The amount of PEG to be conjugated to nanoparticles was calculated based on the ratio of 1 μmol of PEG to 5 μmol of sulphydryl groups on nanoparticles. A 100 mg of PEG750 and 150 mg of PEG5000 were mixed with a 10 mL dispersion of thiolated organosilica nanoparticles and stirred for 16 h at room temperature. After the synthesis, nanoparticles were purified against deionized water, as described above.

2.3. Synthesis of fluorescently labelled Si NPs modified with PEG

For *in vitro* experiments, Atto488 iodoacetamide dye was diluted with 100 μL of DMF and kept at −20 °C. Fluorescently labelled organosilica nanoparticles were synthesised by adding 19 μL of Atto-488 maleimide solution (10 mM in DMSO) to the thiolated nanoparticles solution to make 10 mL in total and stirred for 16 h at room temperature in dark conditions. After the completion of the reaction, fluorescently labelled nanoparticles were purified by dialysis under dark conditions, as described previously. The concentration of Atto-488 was calculated based on the molar ratio of thiols on the surface of the nanoparticles, so 1 μmol of dye was added to 20 μmol of SH groups.

PEGylation of nanoparticles was performed according to previously described protocol (Mun et al., 2016); briefly, 50 mg of PEG750 and 50 mg of PEG5000 were added to 2.5 mL of Atto-488 labelled nanoparticles and stirred for 16 h at room temperature under dark conditions. Purification of nanoparticles was done as described previously.

For the *in vivo* experiments, thiolated nanoparticles were conjugated with Alexa Fluor 750 C5 maleimide for visualisation under IVIS Spectrum CT (Perkin Elmer, USA) *in vivo* imaging system. Alexa fluor 750 C5 maleimide was dissolved in DMSO to a concentration of 10 mM according to the Thermo Fisher protocol. The final concentration of dye in nanoparticle suspension of 1 mM (20 μL of dye was added to19.989 mL of NP dispersion) was reacted for 16 h in the dark at room temperature and followed by purification with dialysis according to the previous steps. Alexa Fluor 750 C5 maleimide labelled nanoparticles were also PEGylated with PEG 5000 Da in the dark at room temperature and purified by dialysis against deionized water.

2.4. Characterisation of synthesised nanoparticles

2.4.1. Ellman's assay

The number of thiol groups on nanoparticles was determined using Ellman's assay(Al Mahrooqi et al., 2018). The freeze-dried nanoparticles (3 mg) were dispersed in a 10 mL phosphate buffer solution (0.5 mol/L, pH 8) for 1 h. Then, 0.5 mL of nanoparticle dispersion was reacted with DTNB for 2 h at room temperature in dark conditions, centrifuged at 13000 rpm for 15 min. The absorbance of the supernatant was measured at 420 nm (Microplate reader Varioscan, Thermo Scientific, USA).

The calibration curve was produced using L-cysteine hydrochloride solution at a concentration range of 0.004 – 0.634 μmol/mL.

2.4.2. Dynamic light scattering

Nanoparticles' size and zeta potential were measured using dynamic light scattering with the Nano-ZS series (Malvern Instruments, U.K.) at 25 °C. Nanoparticles were dispersed in ultrapure water at the ratio of 1:100 with a refractive index of 1.45 at a scattering angle of 173°. The size of nanoparticles is presented as the mean of three replicated hydrodynamic diameters (of three batches) ± standard deviation.

2.4.3. Transmission electron microscopy

The morphological characteristics of nanoparticles were analysed by transmission electron microscopy (JEOL JEM – 1400 Plus). Sample preparation for TEM was as follows: nanoparticles were diluted in ultrapure water to a final concentration of 3 mg/mL and sonicated for 15 min, then 8 μL of sample pipetted on carbon-coated 300 mesh Cu grid and stained with uranyl acetate and left to air-dry under the clean conditions. Samples were visualised at an accelerating voltage of 120 kV.

2.4.4. Raman spectroscopy

Raman spectra were recorded using Raman Spectroscopy & AFM combined system (LabRAM, Horiba, Japan) equipped with $\lambda = 532$ nm laser. Before the experiments a small portion of nanoparticles were freeze-dried using Lyotrap (LTE Scientific, UK) for 3 days, ensuring complete removal of any remaining water (verified by weighing the vial until it reached a stable mass). Nanoparticles in powder form were placed on transparent adhesive tape that adhered to the glass slide. Recorded spectra were analysed and plotted using Origin Pro 2016 software.

2.4.5. Concentration calculations

The stock concentration of nanoparticles was determined in terms of mass per volume. The yield of nanoparticles was assessed gravimetrically after freeze-drying of their aqueous dispersions. Initially, the vial was weighed, and its mass was recorded. Subsequently, a 10 mL nanoparticle dispersion was placed in a vial, weighed, frozen, and then subjected to freeze-drying for 3 days, ensuring complete removal of any remaining water (verified by weighing the vial until it reached a stable mass). After drying, the resulting powder was weighed, and the product's mass was calculated by subtracting the initial vial mass. The concentration was then determined in mg/mL. Across different syntheses, the concentrations varied, but on average, they were around 10–11 mg/mL.

2.4.6. Stability of nanoparticles in physiological media

Nanoparticles were dispersed in three distinct media at the concentration of 100 μg/mL (deionized water, 0.9% sodium chloride solution, and cell culture medium supplemented with 10% FBS). The resulting solution underwent filtration using a syringe filter with a pore size of 0.44 μm. For five days their hydrodynamic size in solution was measured using DLS. Additionally, to understand the role of salt concentration in the Si NP-SH aggregation state, we measured the hydrodynamic size of nanoparticles in solutions with various NaCl concentrations ranging from 100 mM to 6 mM.

2.5. Evaluation of cytocompatibility of organosilica nanoparticles

2.5.1. Cell viability assay

Analysis of cell viability was performed with CellTiter Non-Radioactive Cell Proliferation Assay (MTT) (Promega, USA). HEK293 (Human Embryo Kidney), HPF (human pulmonary fibroblasts), A549 (adenocarcinoma human alveolar basal epithelial cells) and MCF-7 (breast cancer) cells were seeded in 96 well-plate with a density of $5*10^3$ cells per well and incubated at 37 °C, 5% CO_2 overnight. Then, old cell medium (DMEM + 10%FBS + 1% antibiotics) was removed, and nanoparticles' suspensions in cell media were added at concentrations of 0, 10, 50, 100, 200, 400, 800, 1000 μg/mL and incubated for 24, 48 and 72 h at 37 °C humidified atmosphere with 5% CO_2. Cells that were not treated with nanoparticles were denoted as a negative control. After the treatment with nanoparticles, 15 μL of dye solution was added to each well to convert the MTT tetrazolium component into formazan by cell mitochondria for 4 h at 37 °C humidified atmosphere with 5% CO_2,

followed by the addition of 200 μL of Stop Solution to solubilise formed formazan crystals and left for 1 h to react. The absorbance was measured at 570 nm (Microplate reader Varioscan, Thermo Scientific, USA). The following formula was used to calculate the viability:

$$\%CellViability = \frac{Absorbance570oftreatedcells}{Absorbance570ofcontrol} * 100\%$$

2.5.2. Evaluation of hemolytic properties of NPs

The hemolytic properties of nanoparticles were analysed using blood samples that were collected from three healthy volunteers in K2-EDTA vacutainers (Ayset, Turkey); these samples were centrifuged at 1000 rpm for 10 min. Plasma and buffy coats were removed, and red blood cells (RBC) were diluted to prepare a 2% (v/v) RBS solution in PBS. Nanoparticles were dispersed in PBS at 0, 50, 100, 200, 400, 600, 800, and 1000 μg/mL concentrations, then 0.2 mL of nanoparticles suspension was incubated with 0.8 mL RBC solution in an Eppendorf tube for 1 h at room temperature and 37 °C. Then, tubes were centrifuged at 2500 g for 6 min, 200 μL of supernatant was placed on a 96-well plate, and absorbance at 541 nm and 655 nm was recorded. Water and PBS were used as positive and negative controls, respectively. The following formula was used to calculate the percentage of hemolysis:

$$Hemolysis\% = \frac{Asample - Anegativecontrol}{Apositivecontrol - Anegativecontrol} * 100$$

2.6. Cellular permeability using laser scanning confocal microscopy

To study the distribution of the nanoparticles in cells nanoparticles were labelled with Atto-488 maleimide. HEK293 and MCF7 cell lines were grown on 8 well μ-slides (Ibidi, Germany) coated with collagen. Each well had $5*10^4$ (MCF7) and $7*10^4$ (HEK293) cells that were incubated at 37 °C humidified atmosphere with 5% CO_2 for 24 h. Then cells were treated with 400 μg/mL of Si NP- Atto488-SH, Si NP-Atto488-PEG750, and Si NP-Atto 488-PEG 5000 for 2, 4, 6 and 24 h at 37 °C with 5% CO_2. After the cells' exposure to nanoparticles, their excess was removed by washing with PBS 3 times, followed by cell fixation with 4% paraformaldehyde and permeabilisation with 0.2% Triton X-100 solution. Actin filaments and the nucleus were stained with Alexa 555 Phalloidin and DAPI, respectively. After the staining, samples were immersed with Fluoromount-G Mounting Medium (ThermoFisher, USA). Slides were viewed under the laser Scanning Microscope (Carl Zeiss, Germany) with oil immersion objective x63. Z-stack with 0.28–0.30 μm step was taken for each image at the same laser power.

2.7. Slug irritation test

The slug mucosal irritation test was performed according to the previously published protocol(Khutoryanskaya et al., 2008), which is a slightly modified version of the original method introduced by Adriaens and Remon(Adriaens and Remon, 1999; Adriaens and Remon, 2002). *Arion lusitanicus* slugs (Reading, UK) weighing 3–10 g were used for the experiment. The slugs were isolated from their natural environment and kept in pairs in round flat-bottom short glass beakers (19 cm in diameter) for 2 days in the dark before the test. The glass beakers were lined with a paper towel and moisturised with 20 mL of phosphate-buffered saline (PBS) solution. 1% Benzalkonium chloride in PBS and PBS solutions were used as positive and negative controls, respectively. Thiolated and PEGylated (750 and 5000 Da) silica nanoparticle dispersions (0.1% w/v) were prepared by dispersing 6 mg of freeze-dried nanoparticles in 6 mL of PBS. An initial compound, 3-mercaptopropyltrimethoxysilane (MPTS), was also tested for its biocompatibility; a 0.1 % MPTS solution in PBS was prepared. The Whatman filter paper was moisturised with 2 mL of either control or sample solutions and then used to line 9 cm Petri dishes. Each slug was weighed individually before the experiment and then placed into the Petri dish containing the sample being tested. The slugs were kept in Petri dishes covered with lids for 1 h, after which they were taken out, rinsed with 10 mL of PBS, wiped with tissue paper and reweighed. Biocompatibility was assessed based on mucus production (body weight loss), which was calculated according to the following formula:

$$MP = (m_b - m_a)/m_b * 100\%,$$

where MP is the mucus production, m_b is the weight of the slug before the experiment, m_a is the weight of the slug after the experiment. All experiments were carried out in triplicate using different slugs, and the mean MP ± SD value was calculated. The biocompatibility of MPTS and silica nanoparticles were compared to the positive and negative controls and statistical differences were determined using a one-way ANOVA Tukey multiple comparison test.

2.8. Biodistribution of thiolated and PEGylated nanoparticles

Fifty-eight female Balb/C mice aged 8–10 weeks were purchased from the National Center of Biotechnology (Kazakhstan). All mice were housed in the animal facility at the National Laboratory Astana (Kazakhstan) according to Directive 2010/63/EU. The research protocols were approved by the NU-IACUC approval 17/30112020 (22/04/2021 – 21/04/2024). Animals were housed five mice per cage at a temperature of 20–23 °C and 40–60% humidity with constant access to food and water. Before the experiments began, mice were acclimatised for several days in the facility.

For the *in vivo* biodistribution and histology studies, 5 and 3 animals per group were used, respectively; a control (PBS) and treated with fluorescently tagged Si NP-SH and Si NP-PEG5000 groups. Each mouse was anaesthetised with a 5% solution of Isofluorane (1.0 L/min of oxygen) using a gas anesthesia system (Harvard Apparatus, USA). Anaesthetised animals were injected with Si NP-A750-SH and Si NP-A750-PEG5000 nanoparticles at 20 mg/kg(Liu et al., 2011; Mendez et al., 2017; Yu et al., 2012; Liu et al., 2020) 0.9% saline through the tail vein (32G needle size).

2.8.1. Biodistribution

After two hours post-NP injection, animals were deeply anaesthetised and dissected to obtain organs (brain, lung, heart, liver, spleen, kidneys, and GI tract organs). *Ex vivo* fluorescence images of main organs were acquired using IVIS Spectrum CT system (excitation filter 745 nm and emission filter 800) exposure time = 1 s, binning = medium (8), a field of view = 19 × 19 cm, f/ stop = 2. Living Image software 4.3.1 (Perkin Elmer, UK) was used to define and analyse the light emission in the regions of interest (ROIs) quantifying as the Total Radiant Efficiency (TRE, [photons/sec]/[μW/cm^2]).

To reaffirm that the signal from imaging shows the presence of the nanoparticles and not unbound fluorescent dye molecules, organs from mice treated with Si NP-A750-SH were analysed by thermogravimetric analysis (TGA). The sample preparation for TGA included organ homogenisation and freeze-drying to obtain a dry homogeneous powder. 5–9 mg of organ suspension was placed in a ceramic pan and an experiment was performed on a Simultaneous Thermal Analyzer 600 (Perkin Elmer, UK). Experiments were conducted from 30 to 950 °C in a dynamic nitrogen environment with a 10 mL/min flow rate.

2.8.2. Histology

On days 7 and 28, organs were removed from mice for histological analysis. Before dissection, animals were deeply anaesthetised by isoflurane and slaughtered. Organs were taken into the 10% formalin solution. The next day, the formalin solution was refreshed, and after three days, organs were fixated with paraffin, sectioned on microtome and sections attached to glass slides. Cut samples were stained with hematoxylin and eosin, according to Cardiff et al(Cardiff et al., 2014).

2.9. Statistical analysis

All experiments were performed at least in triplicates. Two-way ANOVA and Student's *t*-test were used to confirm the differences between groups for MTT and hemolysis assays.

3. Results and discussion

3.1. Synthesis and characterisation of thiolated organosilica and PEGylated nanoparticles

Self-condensation of (3-mercaptopropyl)trimethoxysilane (MPTS) in an aprotic solvent with a catalyst (NaOH) resulted in the formation of thiolated organosilica nanoparticles (Si NP-SH) as reported previously (Mun et al., 2014). Thiolated nanoparticles were characterised using dynamic light scattering and Ellman's assay. Further, a fraction of thiolated nanoparticles were obtained for functionalisation with polyethylene glycol with molecular weights of 750 Da (Si NP-PEG750) and 5000 Da (Si NP-PEG5000). These specific molecular weights of PEG were previously reported to affect the ability of PEGylated nanoparticles to penetrate various biological membranes. PEGylated nanoparticles also were characterised by DLS and Ellman's assay. PEGylation using PEG5000 led to a significant increase in the size of the nanoparticles; moreover, we can see the reduction of thiol groups from Si NP-SH > Si NP-PEG750 > Si NP-PEG5000 (Table 1). The size distribution of hydrodynamic diameters for thiolated and PEGylated nanoparticles further confirms that PEGylation resulted in larger nanoparticles (Fig. 1c). It is noteworthy to say that the use of a higher molecular weight PEG resulted in the larger size of the nanoparticles.

Moreover, PEGylation changed the surface charge of the nanoparticles, resulting in a reduction of their negative charge when compared to thiolated particles. This observation aligns well with the reduction of sulfhydryl groups upon PEGylation: from 481 ± 79 μmol/g for Si NP-SH to 364 ± 56 μmol/g and 228 ± 99 μmol/g for nanoparticles conjugated with PEG of 750 Da and 5000 Da, respectively (Si NP-PEG750 and Si NP-PEG5000) (Table 1). Raman spectroscopy where the peak associated with the S-H stretch reduced upon PEGylation (2570 cm^{-1}) also confirmed the decrease in thiol groups content (Fig. 1D).

To further investigate the differences in the physical and chemical properties of the nanoparticles, we employed transmission electron microscopy (TEM) to examine the morphological characteristics of PEGylated and thiolated nanoparticles. However, TEM images revealed that the size of dry nanoparticles decreased nearly by half compared to the hydrodynamic diameter of particles determined by DLS. In contrast, the TEM images of thiolated nanoparticles displayed chain-like structures, which also was previously described by Irmukhametova et al (Irmukhametova et al., 2011). Most likely, those chains are formed through intermolecular interactions of SH-groups on the surface of nanoparticles resulting in disulfide bridges (Fig. 1A). PEGylation with PEG5000 eliminated that chain-like arrangement. Further, in this study, we will come across a description of the effect of PEGylation in *in vitro* studies.

Table 1
Physicochemical characteristics of thiolated and PEGylated organosilica nanoparticles.

	Si NP-SH	Si NP-PEG750	Si NP-PEG5000
Hydrodynamic diameter, nm	56 ± 1	55 ± 1	63 ± 1
Diameter, nm (TEM)	29 ± 4	28 ± 5	28 ± 6
PDI	0.140 ± 0.010	0.127 ± 0.008	0.135 ± 0.009
ξ-potential, mV	−45.4 ± 3.0	−34.9 ± 10.8	−28.9 ± 6.5
SH group content, μmol/g	481 ± 79	364 ± 56	228 ± 99

It is well known that the aggregation of nanoparticles in physiological media may lead to changes in their behavior, and more importantly, may result in severe toxicity and even death (Mohammadpour et al., 2019; Li et al., 2020; Avsievich et al., 2020). To assess changes in the size of nanoparticles in different media and understand the role of PEGylation, we measured the size of Si NP-SH, Si NP-PEG750, and Si NP-PEG5000 in three distinct media: deionized water, 0.9% NaCl solution, and cell culture medium with 10% FBS. As shown in Fig. 2, the size of nanoparticles did not change significantly within five days, and the hydrodynamic size remained within an acceptable range for all nanoparticle types in all solutions, except for Si NP-SH in saline. We observed that Si NP-SH formed large aggregates in the saline solution even after filtration. This could be attributed to the salting out effect of NaCl and the poorer colloidal stability of non-PEGylated nanoparticles, a similar effect observed in sulfhydryl-containing proteins (Kang et al., 2021). To determine whether the aggregation of Si NP-SH is dependent on salt concentration, we measured the hydrodynamic size at different salt concentrations. We observed that the aggregation state of Si NP-SH is highly dependent on salt concentration, stabilizing upon reaching a concentration of 25 mM, where nanoparticles seemed to lose the property to aggregate, and their PDI stabilized (see Supplementary Material). Regarding the size of nanoparticles in cell culture media, we observed that Si NP-SH is larger than PEGylated nanoparticles. This difference could be attributed to the formation of a protein corona on the surface of thiolated nanoparticles, and PEGylation is a limiting factor for the deposition of proteins on nanoparticles.

Also, whether the unreacted PEG molecules were successfully removed during the purification process is worth considering. As the purification of nanoparticles plays a significant role in the properties of nanoparticles, we performed prolonged dialysis against deionized water for eight water changes with a dialysis membrane of 12–14 kDa MWCO cut-off. The membrane's pore size was 2–3 times higher than the size of the functionalised nanoparticles, and various groups successfully used this method previously (Lassenberger et al., 2016; Tehrani et al., 2023; Urata et al., 2009). However, the right choice of purification technique highly depends on the type of nanoparticle; for example, the preferred method for metallic nanoparticles is precipitation and magnetic decantation(Lassenberger et al., 2016), while for organic nanoparticles, it is more complicated. Our results show that dialysis effectively removed excess PEG, as evidenced by monodisperse size distribution (PDI < 0.2) (Ways et al., 2018).

3.2. Evaluation of cytocompatibility of organosilica nanoparticles

The next step of this investigation entailed the evaluation of cytotoxicity of the organosilica nanoparticles in four cell lines of cancerous and non-cancerous origin: primary cells from human lung tissue (HPF), lung carcinoma epithelial cells A549, breast cancer cells MCF-7 and epithelial cells from a human embryo kidney HEK293. Cells were treated with Si NP-SH, Si NP-PEG750 and Si NP-PEG5000 for 24, 48 and 72 h at various concentrations from 10 μg/mL to 1000 μg/mL. We observed that nanoparticles caused toxicity in a dose-dependent and cell line-dependent manner. The viability decreased below 70%, which indicates the incompatibility of the material for biomedical application (ISO, 2009), was observed on Si NP-SH at high concentrations (800 – 1000 μg/mL) after 24, 48 and 72 h in all analysed cell lines. However, A549 cell line was more susceptible to Si NP-SH than other cell lines after 48 and 72 h; cell viability decreased at the 200 μg/mL and 100 μg/mL concentrations, respectively (Fig. 3). Cell lines treated with Si NP-PEG5000 also showed dose-dependent effect and viability below 70% observed at concentrations 800 μg/mL and 1000 μg/mL; NPs exhibited greater susceptibility to A549 cell line. In addition, the toxic effect of Si NP-PEG5000 was observed on HEK293 cell lines at 400 μg/mL and higher concentrations (Fig. 3). Interestingly, Si NP-PEG750 exhibited greater toxicity compared to the other two types of nanoparticles. The effect of Si NP-PEG750 on A549 cell lines was similar to the other two,

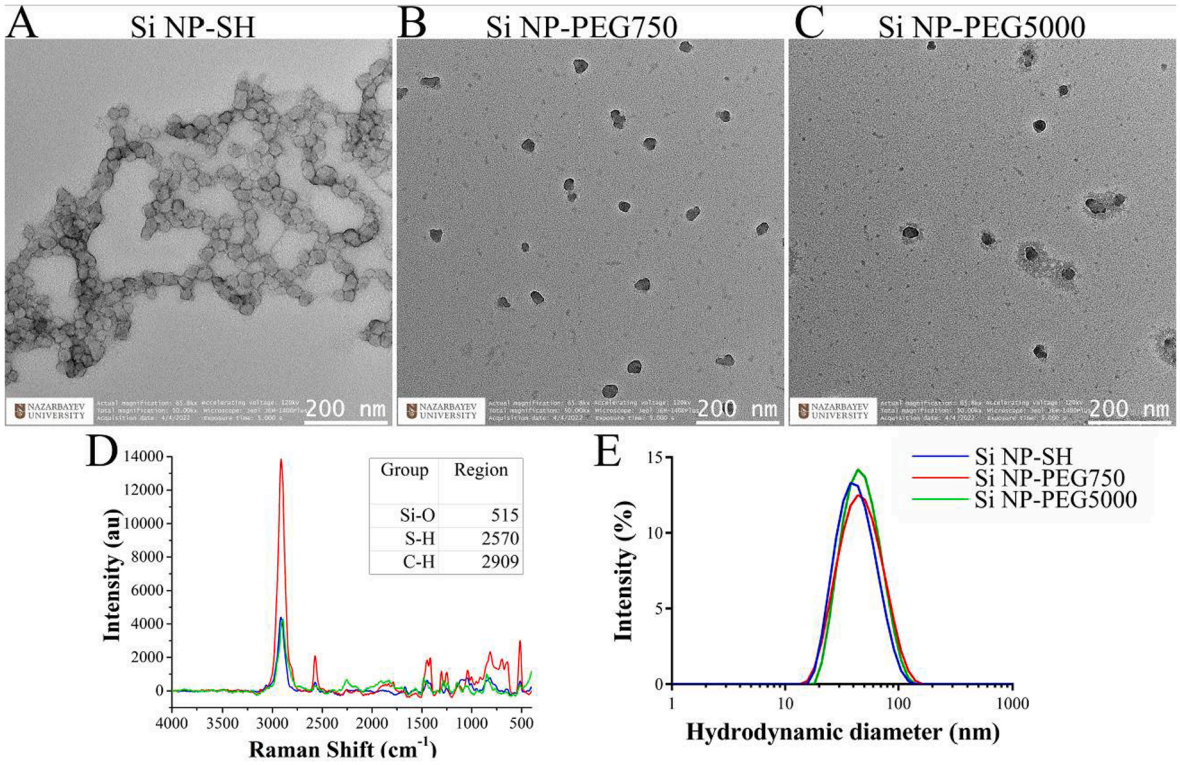

Fig. 1. Physicochemical characteristics of thiolated and PEGylated organosilica nanoparticles: TEM images of A) Si NP-SH, B) Si NP-PEG750 and C) Si NP-PEG5000, D) Raman spectra of NPs with the main Raman signals shown as an insert, and E) hydrodynamic size distribution of NPs in water.

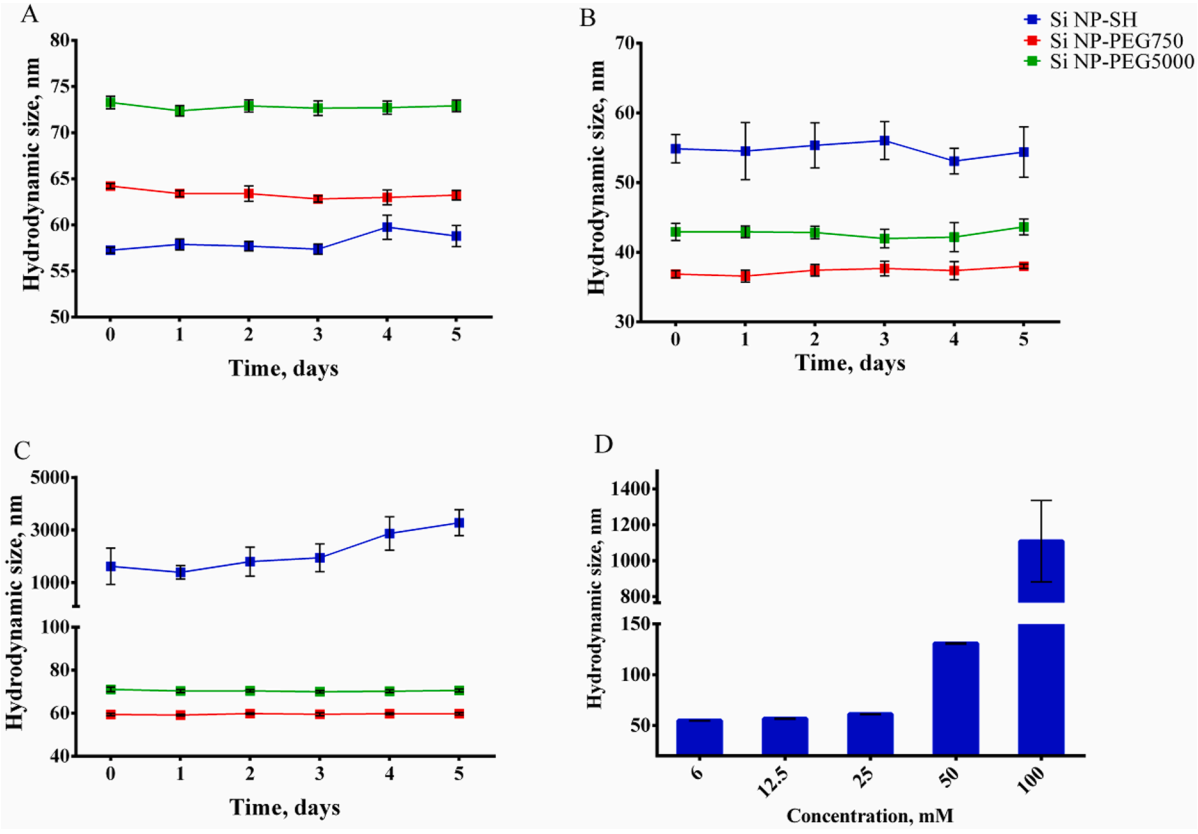

Fig. 2. Hydrodynamic size of Si NP-SH, Si NP-PEG750, and Si NP-PEG5000 measured for 5 days in A) deionized water, B) cell culture medium and C) in 0.9% sodium chloride solution measured for 5 days. D) Size dependence of Si NP-SH in solutions of various concentrations of sodium chloride.

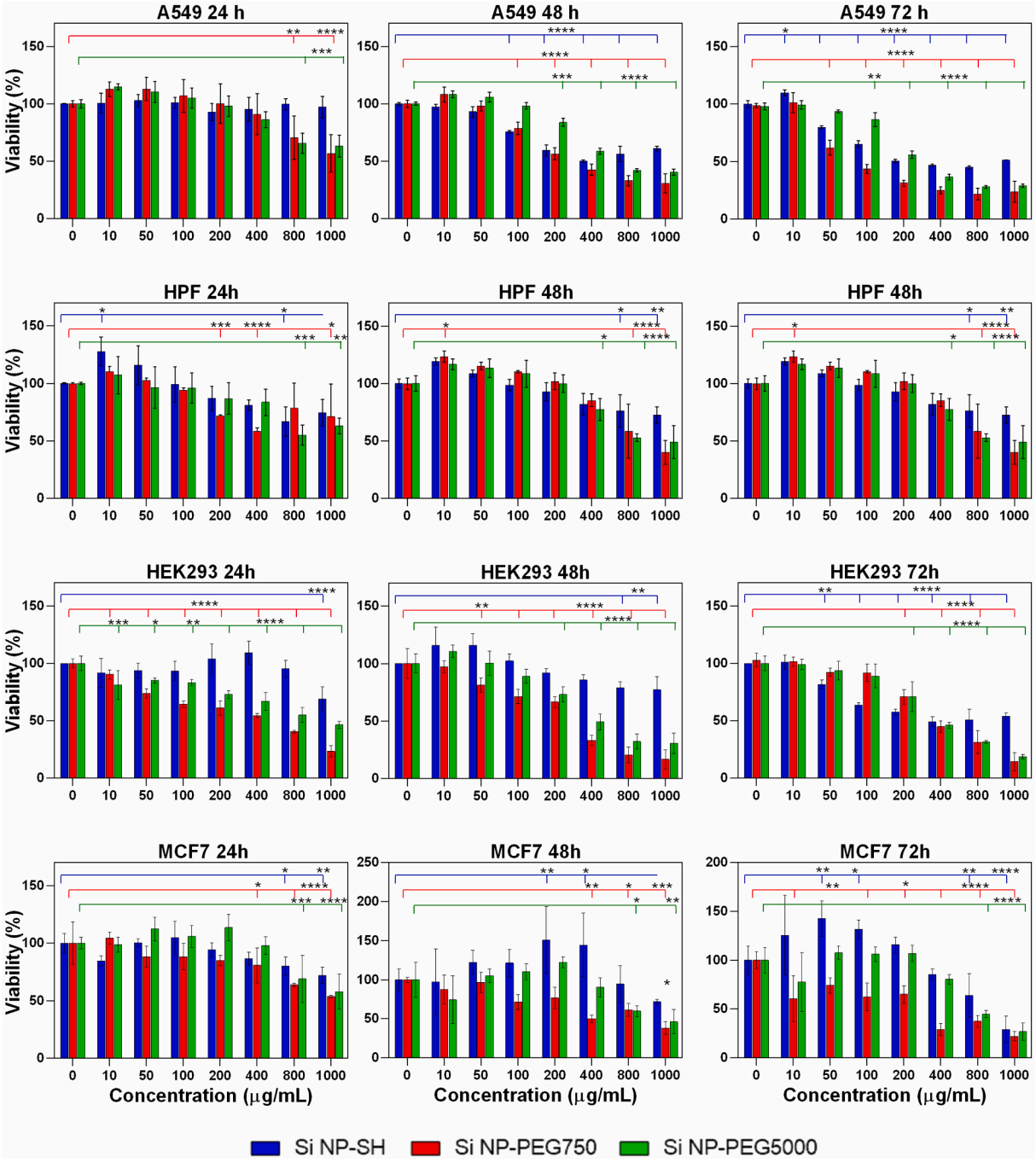

Fig. 3. *In vitro* concentration-dependent cytotoxicity effect of Si NP-SH, Si NP-PEG750 and Si NP-PEG5000 organosilica NPs on four cell lines evaluated with MTT assay. Cells were treated for 24, 48 and 72 h (*P < 0.05;**P ≤ 0.01; ***P ≤ 0.001; ****P ≤ 0.0001).

but after 48 and 72 h of treatment, the viability reduction began at 200 μg/mL and 50 μg/mL, respectively (Fig. 3). In addition, the MCF7 cell line, which was resistant to Si NP-SH and Si NP-PEG5000, demonstrated viability loss after 48 and 72 h (400 μg/mL and 10 μg/mL, respectively).

From the MTT results, we can conclude that Si NP-PEG750 is more destructive to all observed cell types compared to Si NP-SH and SI NP-PEG5000. Generally, nanoparticles are safe for short-term exposure for biomedical applications at low concentrations, between 10 μg/mL to 200–400 μg/mL.

To conduct a more comprehensive evaluation of the cytocompatibility of nanoparticles, we examined hemolytic properties in human blood. As the presence of hemolytic material in the blood may cause damage or loss of red blood cells, eventually increasing levels of free plasma hemoglobin which can induce toxic effects that may stress the kidneys or other organs(Neun et al., 2018). We based our assessment on the ASTM standard(Astm F, 2000), which indicates that the material is considered hemocompatible if a hemolytic index is less than 5%. Red blood cells were treated with nanoparticles for 1 h at 37 °C, and then we collected the hemoglobin from erupted erythrocytes and measured the absorbance. We observed that Si NP-SH caused significant disruption of red blood cells (RBCs) at the 200 μg/mL concentration (3.00 ± 2.26 %, $p < 0.05$) and at higher concentrations further increased the amount of free hemoglobin (Fig. 4E). It suggests that the Si NP-SH causes erythrocyte damage in a concentration-dependent manner. On the other hand, PEGylated nanoparticles showed contradicting results; Si NP-PEG750 affected the RBC integrity at the concentration of 200 μg/mL

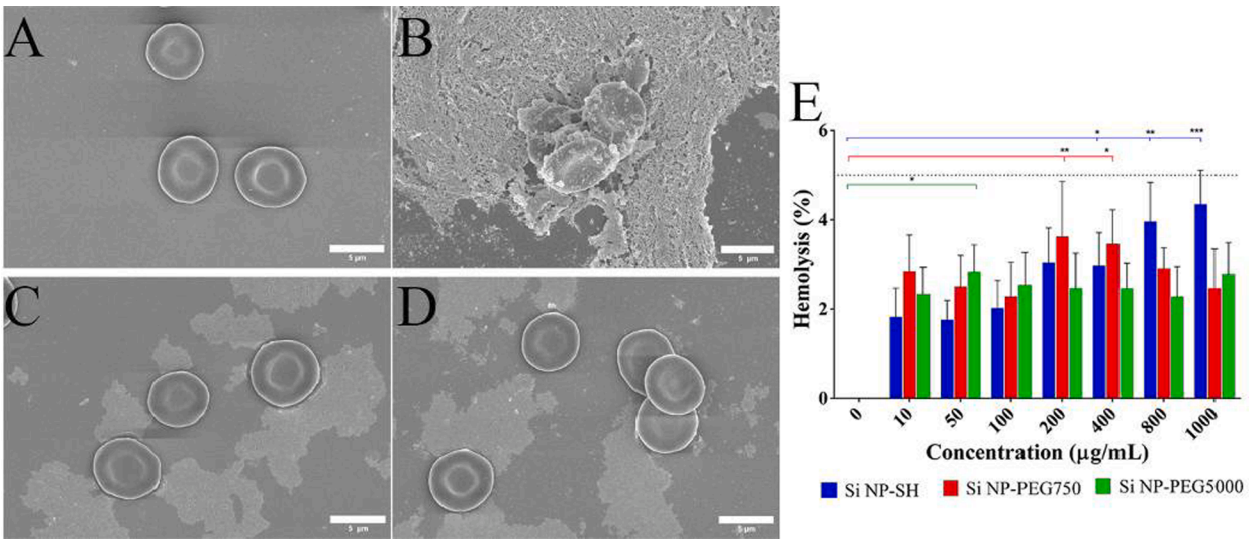

Fig. 4. SEM images of erythrocytes treated with A) PBS, B) Si NP-SH, C) Si NP-PEG750, D) SI NP-PEG5000. Scale bar – 1 μm, and E) results from the hemolysis assay, dotted line corresponds to 5% value (*P < 0.05;**P ≤ 0.01; ***P ≤ 0.001; ****P ≤ 0.0001).

(4.16 ± 3.21 %), and with the increase of the concentration, the hemolytic properties did not rise as for Si NP-SH (Fig. 4e). As for Si NP-PEG5000 the highest free hemoglobin number was observed in samples treated at the concentration 50 μg/mL (2.95 ± 1.23, p < 0.05), and further increase in concentration did not show a significant rise of hemolysis compared to control (Fig. 4E). Nevertheless, the hemolysis assay showed that even the highest values obtained in the experiment fall within the recommended ASTM standard indicators, subsequently, we can consider these nanoparticles hemocompatible. Our hypothesis that Si NP-SH disrupts RBCs at 200 μg/mL and higher concentrations by

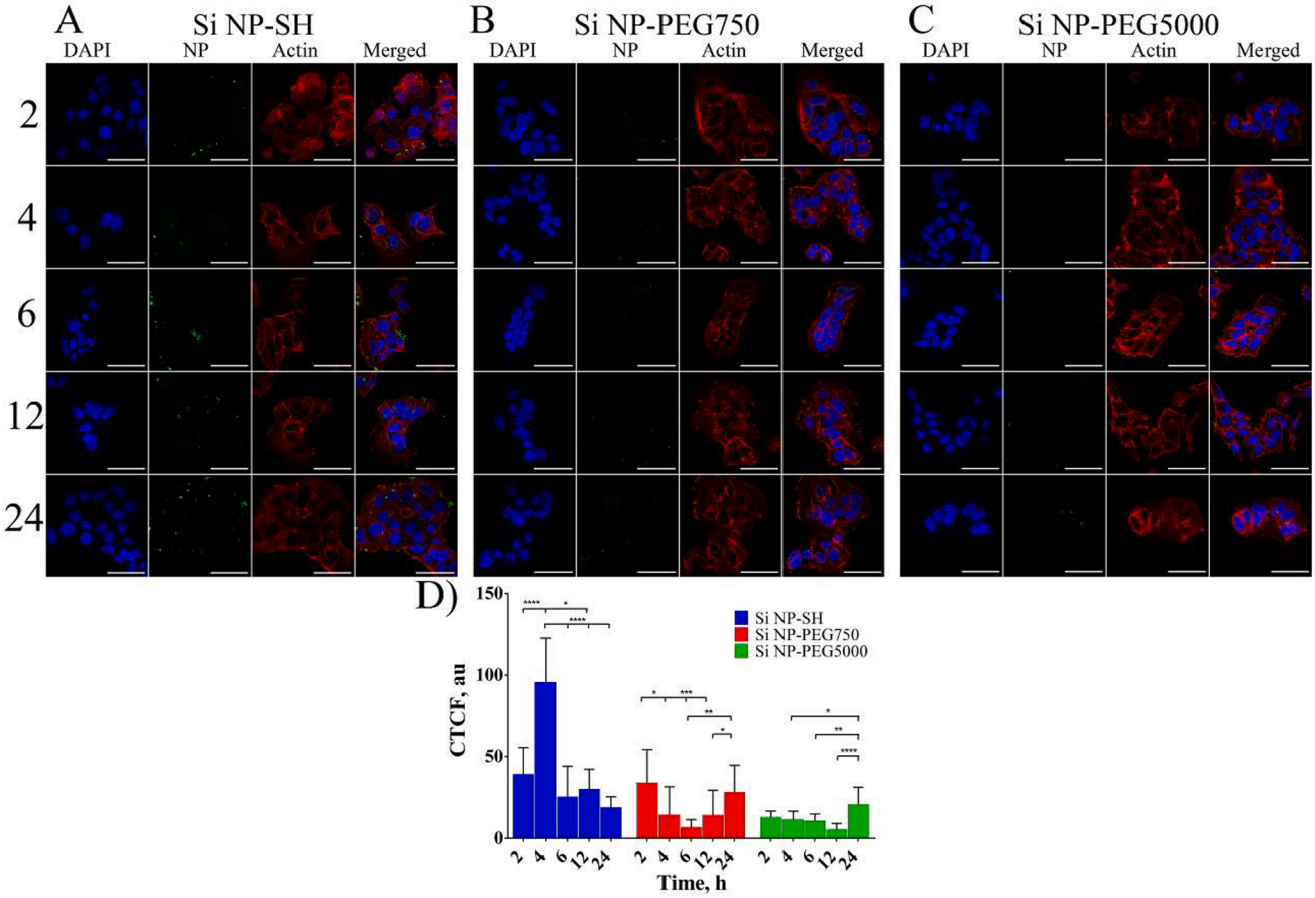

Fig. 5. Permeability of organosilica nanoparticles in MCF7 cell line. Visualisation of internalisation of A) Si NP-SH, B) Si NP-PEG750 and C) Si NP-PEG5000 nanoparticles after 24, 12, 6, 4 and 2 h after the incubation. The blue color represents the nucleus, red-actin filaments and green – nanoparticles. Scale bar – 50 μm; and D) Quantification of corrected fluorescence from the nanoparticles assimilated inside the cell. (*P < 0.05;**P ≤ 0.01; ***P ≤ 0.001; ****P ≤ 0.0001).

forming aggregates around or near erythrocytes and more effectively disrupting the cell membrane was proven by the electron microscopy images. Scanning electron microscope (SEM) images revealed that Si NP-SH forms large aggregates around RBCs, moreover, in some cases; it induced agglutination of erythrocytes, some of which formed clumps (Fig. 4A). While PEGylated nanoparticles behaved completely in different ways, by partially attaching to the erythrocytes and no agglomerates were observed on RBCs (Fig. 4B, C). Nevertheless, one remains clear: nanoparticles can be considered safe for systemic application at low concentrations, as they do not cause erythrocyte lysis. However, the concern about erythrocyte agglutination after the treatment with Si NP-SH remains, which should not be overlooked.

3.3. *In vitro cell uptake of thiolated and PEGylated organosilica nanoparticles*

Based on the results from the MTT assay, the cellular uptake of Si NP-SH, Si NP-PEG750 and Si NP-PEG5000 were studied in MCF7 cell line using laser scanning confocal microscopy. Nanoparticles at the concentration of 400 μg/mL were incubated with cells for 2, 4, 6, 12 and 24 h to see the time-dependent absorption, followed by fixation and staining as described in the methods section. Results revealed that nanoparticles penetrate through the cell membrane in a time-dependent manner. In addition, the ability of Si NP-SH to penetrate through the cell membrane and congregate in the cytoplasm was when compared to PEGylated nanoparticles and after 24 h treatment thiolated nanoparticles formed aggregates inside the cellular cytoplasm (Fig. 5A, 5B and 5C). We propose that at this concentration the nanoparticles may cause viability reduction due to the formation of clusters within and on cells and it agrees with the results obtained from the MTT assay, where a drop in viability was observed at the concentration of 400 μg/mL. In addition, the high molecular weight of PEG increases the time for nanoparticles penetration through the cell membrane (Fig. 5C). For Si NP-PEG5000 it took nearly 6 h to be visualised inside the cell, while for Si NP-SH and Si NP-PEG750, it took at least 2 h. Further, we needed to quantify the approximate values of NP internalised inside the cells, for that, we correlated the total green fluorescence in cells with ImageJ software by subtracting the area of selected cells multiplied by the background mean grey value from the integrated density value (Fig. 5D). Results showed that Si NP-SH has the highest internalisation capability and by the 4th hour, we observed the highest fluorescent intensity inside the cellular cytoplasm, while for PEGylated nanoparticles, the highest fluorescent intensity was observed after the 24-hour incubation. We assume that thiolated nanoparticles rapidly penetrate through the cellular membrane and are slowly released from the cell over time, while PEGylated nanoparticles take more time to internalise. Our findings confirm previous studies reporting that PEGylation of nanoparticles lowers their adsorption by cell lines(Pelaz et al., 2015; Kim et al., 2021). PEGylated nanoparticles require a longer time to internalise through the cell membrane and thus we observed cell death in the MTT assay after 48 and 72 h at high concentrations. While thiol groups on the surface of Si NP-SH may interfere with the transmembrane proteins on the cell surface and increase the permeability(Hock et al., 2022).

3.4. *Slug mucosal irritation (SMI) test*

As one of the potential applications of organosilica nanoparticles is transmucosal drug delivery, we performed slug mucosal irritation (SMI) assay of Si NP-SH, SI NP-PEG750 and Si NP-PEG5000 nanoparticles and MPTS (1 mg/mL) using *Arion lusitanicus* terrestrial slugs. PBS and benzalkonium chloride (BAC) served as negative and positive controls, respectively.

When exposed to PBS solutions, slugs were noted to be comfortable with the environment, releasing clear mucus, and remaining steady on their foot, not moving intensively. However, when they were placed in the Petri dish containing 1% BAC, a rapid release of thick yellow mucus was observed, which indicates the irritating nature of BAC. Additionally, these slugs moved very actively inside the Petri dish, trying to avoid contact with an irritant chemical.

In this experiment, the mucus production was 19.3 ± 1.6 % and 1.8 ± 0.8 % for positive and negative controls, respectively (Fig. 6). These parameters are slightly lower than previously reported 33 ± 14 % and 3.6 ± 1.0 % by Khutoryanskaya et al.(Khutoryanskaya et al., 2008). This discrepancy can be explained by the different slug species used for the experiments: *Arion lusitanicus* (in the current work) and *Limax flavus* (Khutoryanskaya et al., 2008).

3-mercaptopropyltrimethoxysilane, the precursor of silica nanoparticles, is a “harmful and dangerous to the environment substance”, according to its MSDS (EU directives 67/548/EEC or 1999/45/EC classification). 0.1 % MPTS caused 9.2 ± 2% mucus release in the slug mucosal irritation test, which determines it as “a risk of serious damage” material(Dhondt et al., 2006; Adriaens et al., 2008). Similar effect was observed after the addition of BAC (positive control) which caused the production of 8 ± 0.7 % mucus, while pure MPTS caused a slug mortality within 10 min, which demonstrates its toxic nature(Dhondt et al., 2006; Adriaens et al., 2008).

Thiolated silica nanoparticles (0.1% w/v in PBS) were determined as non-irritant, producing 1.4 ± 1.0 % of mucus in the SMI assay (Fig. 6A). PEGylated (750 and 5000 Da) silica nanoparticles were also found to be non-irritant, with 1.3 ± 1 % and 1.2 ± 1 % of mucus production, respectively (Fig. 6A, C). Consequently, PEGylated nanoparticles have been widely used in drug delivery applications(Zhang et al., 2008; Danquah et al., 2010; Jalali et al., 2011; Bayard et al., 2013; Devanand Venkatasubbu et al., 2013). In the current experiment, slugs exposed to both thiolated and PEGylated nanoparticles released clear mucus and the ability of these silica nanoparticles to irritate mucosa was found to be as low as the negative control (PBS), with no statistical difference ($p = 0.86$, one-way ANOVA Tukey test).

3.5. *In vivo biodistribution and toxicity profile of organosilica nanoparticles*

Results from the previous experiments did not demonstrate any significant cytotoxicity of nanoparticles *in vitro*; therefore, the next logical step was the investigation of nanoparticle toxicity in animal models. Prior to prolonged *in vivo* studies, we wanted to assess the biodistribution of nanoparticles and their histological impact on main animal organs. To minimise the use of animals, we decided to investigate two types of organosilica nanoparticles that exhibited the most conflicting results although showed less toxicity on MTT assay: Si NP-SH and Si NP-PEG5000.

For this purpose, the nanoparticles were conjugated with a fluorescent dye (Alexa Fluor 750 C5 maleimide) to allow their visualisation under the IVIS spectrum imaging station. Fluorescent labelling of the nanoparticles did not result in a significant increase of their size. As indicated earlier, PEGylation slightly increased the size of nanoparticles but importantly it remained below the sub-100 nm (supplementary materials).

The main aim that we prioritised was to analyse the biodistribution of nanoparticles. Thus, after the injection of Si NP-SH and Si NP-PEG5000 nanoparticles into mice’s tail veins the animals were allowed to sleep under anesthesia and were then euthanised according to the ethical regulations of the university. The main organs such as brain, heart, lungs, liver, kidneys, spleen and GI tract organs were removed and analysed for the presence of fluorescent signal on the IVIS Spectrum CT system. We observed fluorescence signal from the thiolated nanoparticles in the lungs till day 7 then the fluorescent signal disappeared and appeared in the spleen (day 14 and 28) and stomach (day 28) (Fig. 7). One of the challenges with a fluorescent dye is photobleaching, and to ensure that the absence of signal in the lung was not due to fluorescence loss we performed the thermogravimetric analysis

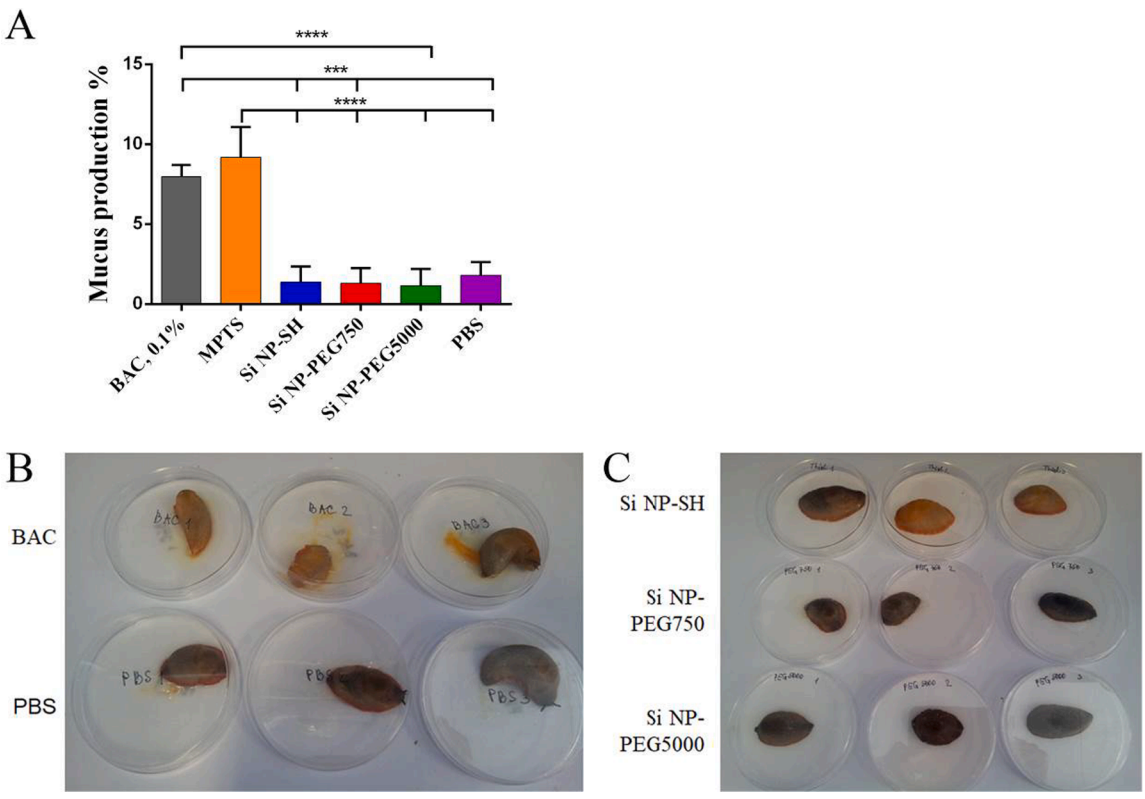

Fig. 6. A) Slug mucosal irritation test results show mucus production by slugs in response to controls, MPTS, Si NP-SH, Si NP-PEG750 and Si NP-PEG5000 nanoparticles. Slugs exposed to control group B) BAC and PBS and experimental group C) Si NP-SH, Si NP-PEG750 and Si NP-PEG5000 nanoparticle solutions.

(TGA), hoping to see that there is no difference in mass between the control and treated groups. The results from TGA confirmed that nanoparticles did not remain in the lung (supplementary materials).

While fluorescence from PEGylated nanoparticles on day 0 was seen only in the liver, then signals appeared in the kidney (day 3), spleen (day 7) and stomach. However, the signal remains in the spleen until day 28, while other organs show no nanoparticles present. After 3 and 7 days of exposure to Si NP-PEG5000 nanoparticles, they appeared in the kidney, which can suggest that part of the nanoparticles excreted through the renal clearance route. Interestingly, He et al (2011) also reported evidence of renal excretion of PEGylated silica nanoparticles, however, in their work, they observed tetraethyl orthosilicate (TEOS) nanoparticles that were conjugated with –OH, –COOH and PEG and all types left the body via kidney, though nanoparticles with –OH and –COOH groups showed higher uptake by the liver(Hadipour Moghaddam et al., 2019). In another study, silica particles of smaller sizes escaped from being captured by liver and spleen tissues and were slowly biodegraded. Furthermore, PEGylation of nanoparticles protects NPs from being trapped in the liver, spleen, and lung tissue(He et al., 2011; Borak et al., 2012).

From the distribution studies, we can see that thiolated nanoparticles adhere to the mucosal tissue as was reported previously *in ex vivo* studies (Mun et al., 2016; Ways et al., 2020). Therefore, we can consider thiolated nanoparticles for the drug delivery systems to respiratory tract, urinary tract, or reproductive system organs, as they are lined with mucosal tissues.

Regarding the excretion of nanoparticles from the body, we observed fluorescence from thiolated nanoparticles on the third and seventh days in the GI tract, liver and the stomach and intestine lining, which suggests hepatobiliary clearance(Poon et al., 2019; Souris et al., 2010). The fluorescent signal from PEGylated nanoparticles is also seen in the kidneys, suggesting nanoparticle elimination happens by the hepatobiliary and renal pathways.

We sacrificed another group of mice for histological analysis to assess any tissue damage caused by the nanoparticles. The structure of the studied organs after intravenous administration of nanoparticles did not change significantly. The structure of the liver was preserved with the thin capsule, represented by fibrous connective tissue. The lobules retained their structure as a hexagonal prism, which is based on hepatocytes arranged in strands. Kuepfer cells, located inside the sinusoidal capillary, attach to the endothelium of the sinusoidal capillary. In the liver, we observed lymphocyte infiltrations on days 7 and 28 for both nanoparticles (Fig. 8).

The light microscopy images of the spleen revealed that composition remained regular with distinct white and red pulp made of distinct cells after four weeks after NP exposure. The main drawback of nanoparticles may be the destruction of the spleen composition(Awaad, 2015). We observed an increased number of small and medium-sized lymphocytes in the mantle zone of the lymphoid in all groups. After a week after NP injection, we can see megakaryocytes in the groups treated with both NP types and their number increased after 4 weeks. The number of megakaryocytes was higher in the spleen of mice treated with Si NP-A750-PEG5000. The data agrees with previous studies on mesoporous silica, suggesting that the spleen and liver are the main organs that trap nanoparticles(Yu et al., 2018; Chan et al., 2017; Rascol et al., 2018; Yang et al., 2019).

Due to the small size of nanoparticles, the possible elimination pathway via the kidney was also considered in the study; therefore, a histological evaluation of kidney tissue was performed. Moreover, we observed signals in the kidney in mice treated with Si NP-PEG5000. The observations showed that there were no significant destructions of kidney architecture. Nevertheless, we see expressed lymphocytic infiltration in the cortical area and medulla of kidneys on days 7 and 28.

No necrotic areas were observed in histological samples, suggesting that nanoparticles did not cause toxicity. Our finding is in agreement with previously published data showing good tissue biocompatibility of silica nanoparticles after *in vivo* oral administration and intravenous injection into mice. It was also demonstrated that silica nanoparticles

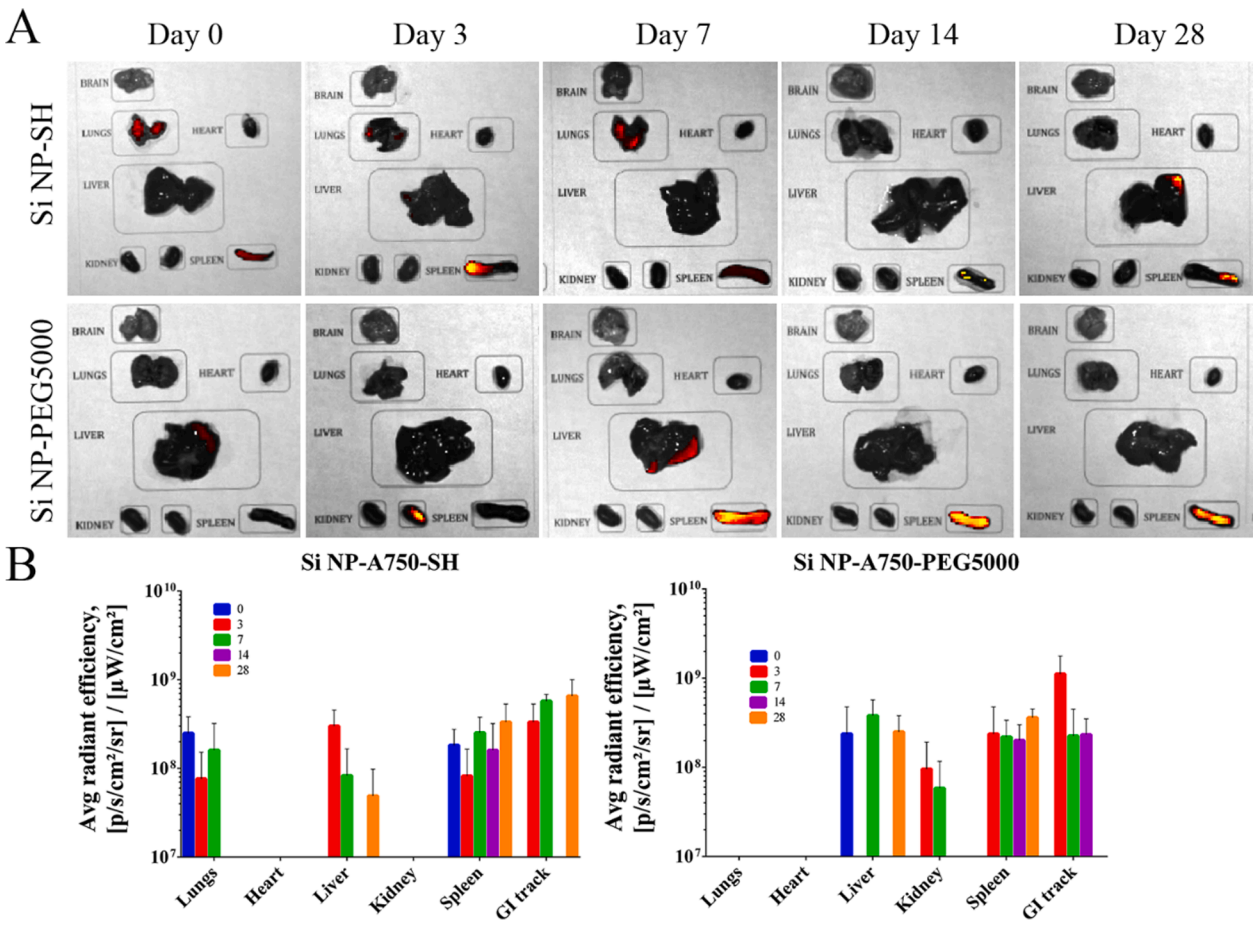

Fig. 7. *In vivo* distribution of organosilica nanoparticles: A) Mice were IV injected with Si NP-SH and Si NP-PEG5000 nanoparticles at the concentration of 10 mg/kg of animal, after 2 h, 3, 7, 14 and 28 days organs were dissected and imaged on IVIS Spectrum CT system for fluorescence; B) calculated average radiant efficiency ($\mu W/cm^2$) from the captured images.

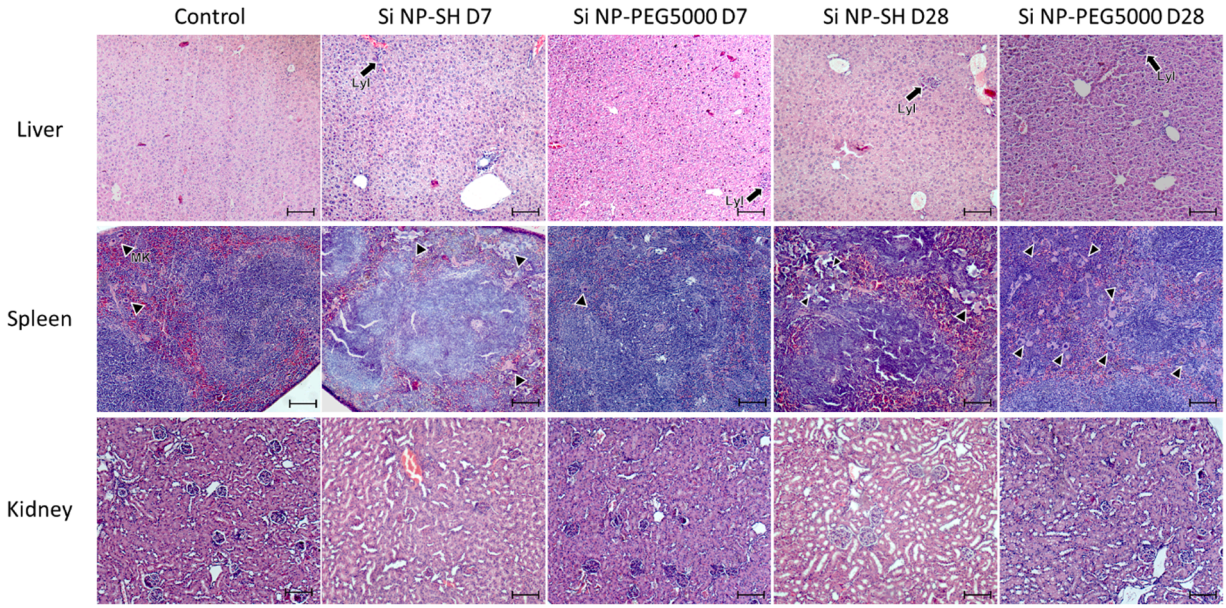

Fig. 8. Light microscopy images of the liver, spleen and kidney slices stained with haematoxylin and eosin after the injection with Si NP-SH and Si NP-PEG5000. Organs were harvested after a week and 4 weeks post-IV injection. Triangles (MK) show megakaryocytes, an arrow (LyI) - lymphocyte infiltration. Scale bar – 100 µm.

can be safely administrated via hypodermic and intramuscular routes(Fu et al., 2013). Liu and co-workers also reported the low toxicity of silica nanoparticles injected intravenously as a single dose or repeated administration(Liu et al., 2011). Additionally, there was no evident embryo toxicity observed when studying the toxicity of silica nanoparticles in zebrafish, demonstrating a low risk of using these particles for biomedical application(Fent et al., 2010).

4. Conclusion

In this study, we performed a comprehensive toxicological study investigating the *in vitro* and *in vivo* toxicological properties and biodistribution of thiolated and PEGylated nanoparticles (Si NP-SH, Si NP-PEG750 and Si-NP-PEG5000) in various cell cultures, human blood and animals using spectroscopy, optical imaging and electron microscopy techniques. Our aim was to make a valuable contribution to ongoing research on organosilica nanoparticles and collaboratively, with the scientific community, determine the appropriate applications for both modified and non-modified nanoparticles. As seen from the results of *in vitro* studies, those nanoparticles can be used as a delivery system or imaging tools if properly functionalised. It is worth mentioning that most of the viability tests on nanoparticles are performed at the concentration range of 0–100 μg/mL(Park et al., 2016; Niu et al., 2016; Guo et al., 2015; Lee et al., 2020) and in our study, we did not observe cytotoxicity at concentrations of 100 μg/mL and bellow for all NP types. Moreover, the viability of A549 and MCF-7 cell lines did not fall below 70% even at the concentration of 400 μg/mL after 24 h of nanoparticle exposure. From these findings, we can conclude that the toxicity of nanoparticles is concentration, exposure time and nanoparticle type dependent. Besides, it is important to consider the molecular mass of PEG for PEGylation; as our work demonstrates that Si NP-PEG750 showed increased toxicity compared to Si NP-SH and Si NP-PEG5000.

In addition, we observed that thiolated organosilica nanoparticles have better and faster internalisation than their PEGylated counterparts and that PEG with a higher molecular weight takes a longer time to internalise. This suggested that the size of nanoparticles is a more limiting factor in cell internalisation than their surface properties. Moreover, the ability of thiolated nanoparticles to adhere to the cell surface makes it a promising candidate for mucosal drug delivery systems.

The histological data demonstrates mild effects of both types of nanoparticles on the spleen and liver, which was expected, taking into account the elimination pathways of those nanoparticles. No major damage to kidney structure and no necrotic tissues were observed after the exposure to both types of nanoparticles.

The results of our comprehensive study not only complement previous data about the potential use of organosilica nanoparticles but manifest MPTS-based nanoparticles as a competitive type of nanoparticles for biomedical applications. Thiolated nanoparticles, on the other hand, could be further modified with various ligands and targeting agents and chemistry similar to the PEGylation may be applied, making MPTS-based nanoparticles advantageous over other silica particles.

We believe that this study adds not only to understanding the potential application of organosilica nanoparticles in the biomedical field but also has an impact on developing comprehensive analysis methods for any nanoparticles that can be used for medical application. The methods to analyse nanotechnology tools for biomedical applications should be standardised, and the National Cancer Institute attempted to encompass all the methods; however, due to the range of types of nanoparticles, the data should be constantly updated (Institute, 2023). However, the collected protocols provide insights into the significant studies that need to be conducted, and further investigation of organosilica nanoparticles is needed.

CRediT authorship contribution statement

Balnur A. Zhaisanbayeva: Investigation, Methodology, Formal analysis, Writing – original draft preparation. **Ellina A. Mun:** Conceptualization, Supervision, Writing – review & editing. **Leila Ulmanova:** Investigation. **Zarina Zhunissova:** Investigation. **Bauyrzhan Umbayev:** Investigation, Writing – review & editing. **Farkhad Olzhayev:** Investigation. **Ivan A. Vorobjev:** Writing – review & editing, Supervision. **Gonzalo Hortelano:** Writing – review & editing, Supervision, Resources, Funding acquisition. **Vitaliy V. Khutoryanskiy:** Conceptualization, Supervision, Writing – review & editing.

Declaration of Competing Interest

The authors declare that they have no known competing financial interests or personal relationships that could have appeared to influence the work reported in this paper.

Data availability

Data will be made available on request.

Acknowledgements

The authors wish to thank Core Facilities of Nazarbayev University for assistance with electron and optical microscopes; Sholpan Askarova (head of the Laboratory of Bioengineering and regenerative medicine), who allowed us to use animal facilities. This research has been funded by the Science Committee of the Ministry of Science and Higher Education of the Republic of Kazakhstan (Grant No. AP13068353). VVK acknowledges the financial support provided by the Royal Society for his Industry Fellowship (IF/R2/222031).

All the experiments using human material (blood) were performed in accordance with the principles of Nazarbayev University Institutional Research Ethics Committee (IREC). IREC is responsible for oversight of ethical standards while conducting human subject research at the University.

All experiments using animals (mice) were performed in accordance with the principles of the Institutional Animal Care and Use Committee of Nazarbayev University (IACUC). IACUC is responsible for oversight of ethical standards while conducting animal subject research at the University.

All experiments using hazardous materials were performed in accordance with the principles of the Bio and Chemical Safety Committee of Nazarbayev University.

1. **NU-IREC approval 355/11012021** (01/03/2021 – 28/02/2022, extended to 28/02/2023);
2. **NU-IACUC approval 17/30112020** (22/04/2021 – 21/04/2024);
3. **NU-BCSC approval 34/02042021** (21/05/2021).

Appendix A. Supplementary data

Supplementary data to this article can be found online at https://doi.org/10.1016/j.ijpharm.2024.123852.

References

Adriaens, E., Remon, J.P., 1999. Gastropods as an Evaluation Tool for Irritating Potency of Absorbtion Enhancers and Drugs. Pharm. Res. 16, 8.

Adriaens, E., Remon, J.P., 2002. Evaluation of an alternative mucosal irritation test using slugs. Toxicol. Appl. Pharmacol. 182 (2), 169–175. https://doi.org/10.1006/taap.2002.9444.

Adriaens, E., Bytheway, H., De Wever, B., et al., 2008. Successful prevalidation of the slug mucosal irritation test to assess the eye irritation potency of chemicals. Toxicol. Vitr. 22 (5), 1285–1296. https://doi.org/10.1016/j.tiv.2008.02.018.

Ahmadi, A., Sokunbi, M., Patel, T., Chang, M.W., Ahmad, Z., Singh, N., 2022. Influence of Critical Parameters on Cytotoxicity Induced by Mesoporous Silica Nanoparticles. Nanomaterials. 12 (12) https://doi.org/10.3390/nano12122016.

Al Mahrooqi, J.H., Mun, E.A., Williams, A.C., Khutoryanskiy, V.V., 2018. Controlling the Size of Thiolated Organosilica Nanoparticles. Langmuir. 34 (28), 8347–8354. https://doi.org/10.1021/acs.langmuir.8b01556.

Al-shuwaili, Z.A.H., Homayouni Tabrizi, M., Ghobeh, M., 2023. Preparation of oxypeucedanin-loaded PLGA-chitosan nanoparticles: Cytotoxicity, apoptosis induction, and anti-angiogenic effects. J. Drug. Deliv. Sci. Technol. 82 (February), 104303 https://doi.org/10.1016/j.jddst.2023.104303.

Amin, H., Amin, M.A., Osman, S.K., Mohammed, A.M., Zayed, G., 2023. International Journal of Biological Macromolecules Chitosan nanoparticles as a smart nanocarrier for gefitinib for tackling lung cancer : Design of experiment and in vitro cytotoxicity study. Int. J. Biol. Macromol. 246 (February), 125638 https://doi.org/10.1016/j.ijbiomac.2023.125638.

ASTM F 756-00. Standard practice for assessment of hemolytic properties of materials. Philadelphia. Am. Soc. Test. Mater. 2000;(January):5. doi:10.1520/F0756-13. Copyright.

Avsievich, T., Tarakanchikova, Y., Zhu, R., et al., 2020. Impact of nanocapsules on red blood cells interplay jointly assessed by optical tweezers and microscopy. Micromachines. 11 (1), 1–12. https://doi.org/10.3390/mi11010019.

Awaad, A., 2015. Histopathological and immunological changes induced by magnetite nanoparticles in the spleen, liver and genital tract of mice following intravaginal instillation. J. Basic. Appl. Zool. 71, 32–47. https://doi.org/10.1016/j.jobaz.2015.03.003.

Bayard, F.J.C., Thielemans, W., Pritchard, D.I., et al., 2013. Polyethylene glycol-drug ester conjugates for prolonged retention of small inhaled drugs in the lung. J. Control. Release. 171 (2), 234–240. https://doi.org/10.1016/j.jconrel.2013.07.023.

Borak, B., Biernat, P., Prescha, A., Baszczuk, A., Pluta, J., 2012. In vivo study on the biodistribution of silica particles in the bodies of rats. Adv. Clin. Exp. Med. 21 (1), 13–18.

Cardiff, R.D., Miller, C.H., Munn, R.J., 2014. Manual hematoxylin and eosin staining of mouse tissue sections. Cold. Spring. Harb. Protoc. 2014 (6), 655–658. https://doi.org/10.1101/pdb.prot073411.

Chan, W.T., Liu, C.C., Chiau, J.S.C., et al., 2017. In vivo toxicologic study of larger silica nanoparticles in mice. Int. J. Nanomedicine. 12, 3421–3432. https://doi.org/10.2147/IJN.S126823.

Chen, Y.P., Chou, C.M., Chang, T.Y., et al., 2022. Bridging Size and Charge Effects of Mesoporous Silica Nanoparticles for Crossing the Blood-Brain Barrier. Front. Chem. 10 (June), 1–17. https://doi.org/10.3389/fchem.2022.931584.

Cheng, C.S., Liu, T.P., Chien, F.C., Mou, C.Y., Wu, S.H., Chen, Y.P., 2019. Codelivery of Plasmid and Curcumin with Mesoporous Silica Nanoparticles for Promoting Neurite Outgrowth. ACS. Appl. Mater. Interfaces. 11 (17), 15322–15331. https://doi.org/10.1021/acsami.9b02797.

Danquah, M., Fujiwara, T., Mahato, R.I., 2010. Self-assembling methoxypoly(ethylene glycol)-b-poly(carbonate-co-l-lactide) block copolymers for drug delivery. Biomaterials. 31 (8), 2358–2370. https://doi.org/10.1016/j.biomaterials.2009.11.081.

Decan, N., Wu, D., Williams, A., et al., 2016. Characterization of in vitro genotoxic, cytotoxic and transcriptomic responses following exposures to amorphous silica of different sizes. Mutat. Res. Toxicol. Environ. Mutagen. 796, 8–22. https://doi.org/10.1016/J.MRGENTOX.2015.11.011.

Devanand Venkatasubbu, G., Ramasamy, S., Avadhani, G.S., Ramakrishnan, J.K., 2013. Surface modification and paclitaxel drug delivery of folic acid modified polyethylene glycol functionalized hydroxyapatite nanoparticles. Powder. Technol. 235, 437–442. https://doi.org/10.1016/j.powtec.2012.11.003.

Dhondt, M.M.M., Adriaens, E., Pinceel, J., Jordaens, K., Backeljau, T., Remon, J.P., 2006. Slug species- and population-specific effects on the end points of the Slug Mucosal Irritation test. Toxicol. Vitr. 20 (4), 448–457. https://doi.org/10.1016/j.tiv.2005.09.002.

Ding, L., Yao, C., Yin, X., et al., 2018. Size, Shape, and Protein Corona Determine Cellular Uptake and Removal Mechanisms of Gold Nanoparticles. Small. 14 (42), 1801451. https://doi.org/10.1002/smll.201801451.

Dolai, J., Mandal, K., Jana, N.R., 2021. Nanoparticle Size Effects in Biomedical Applications. ACS. Appl. Nano. Mater. 4 (7), 6471–6496. https://doi.org/10.1021/acsanm.1c00987.

Domac, B.H., AlKhatib, S., Zirhli, O., et al., 2020. Effects of PEGylated Fe–Fe3O4 core-shell nanoparticles on NIH3T3 and A549 cell lines. Heliyon. 6 (1) https://doi.org/10.1016/j.heliyon.2019.e03124.

Emam, S.E., Abu Lila, A.S., Elsadek, N.E., et al., 2019. Cancer cell-type tropism is one of crucial determinants for the efficient systemic delivery of cancer cell-derived exosomes to tumor tissues. Eur. J. Pharm. Biopharm. 145, 27–34. https://doi.org/10.1016/j.ejpb.2019.10.005.

Eswari, K.M., Asaithambi, S., Karuppaiah, M., et al., 2022. Green synthesis of ZnO nanoparticles using Abutilon Indicum and Tectona Grandis leaf extracts for evaluation of anti-diabetic, anti-inflammatory and in-vitro cytotoxicity activities. Ceram. Int. 48 (22), 33624–33634. https://doi.org/10.1016/j.ceramint.2022.07.308.

Fent, K., Weisbrod, C.J., Wirth-Heller, A., Pieles, U., 2010. Assessment of uptake and toxicity of fluorescent silica nanoparticles in zebrafish (Danio rerio) early life stages. Aquat. Toxicol. 100 (2), 218–228. https://doi.org/10.1016/j.aquatox.2010.02.019.

Fiandra, L., Bonfanti, P., Piunno, Y., et al., 2020. Hazard assessment of polymer-capped CuO and ZnO nanocolloids: A contribution to the safe-by-design implementation of biocidal agents. NanoImpact. 17 https://doi.org/10.1016/j.impact.2019.100195.

Fu, C., Liu, T., Li, L., Liu, H., Chen, D., Tang, F., 2013. The absorption, distribution, excretion and toxicity of mesoporous silica nanoparticles in mice following different exposure routes. Biomaterials. 34 (10), 2565–2575. https://doi.org/10.1016/j.biomaterials.2012.12.043.

Ghaferi, M., Asadollahzadeh, M.J., Akbarzadeh, A., Shahmabadi, H.E., Alavi, S.E., 2020. Enhanced efficacy of PEGylated liposomal cisplatin: In vitro and in vivo evaluation. Int. J. Mol. Sci. 21 (2) https://doi.org/10.3390/ijms21020559.

Guo, C., Xia, Y., Niu, P., et al., 2015. Silica nanoparticles induce oxidative stress, inflammation, and endothelial dysfunction in vitro via activation of the MAPK/Nrf2 pathway and nuclear factor-κB signaling. Int. J. Nanomedicine. 10, 1463–1477. https://doi.org/10.2147/IJN.S76114.

Hadipour Moghaddam, S.P., Mohammadpour, R., Ghandehari, H., 2019. In vitro and in vivo evaluation of degradation, toxicity, biodistribution, and clearance of silica nanoparticles as a function of size, porosity, density, and composition. J. Control. Release. 311–312 (May), 1–15. https://doi.org/10.1016/j.jconrel.2019.08.028.

He, Q., Zhang, Z., Gao, F., Li, Y., Shi, J., 2011. In vivo biodistribution and urinary excretion of mesoporous silica nanoparticles: Effects of particle size and PEGylation. Small. 7 (2), 271–280. https://doi.org/10.1002/smll.201001459.

Hock, N., Racaniello, G.F., Aspinall, S., Denora, N., Khutoryanskiy, V.V., Bernkop-Schnürch, A., 2022. Thiolated Nanoparticles for Biomedical Applications: Mimicking the Workhorses of Our Body. Adv. Sci. 9 (1), 1–24. https://doi.org/10.1002/advs.202102451.

Ilbasmis-Tamer, S., Turk, M., Evran, Ş., Boyaci, I.H., Ciftci, H., Tamer, U., 2023. Cytotoxic, apoptotic and necrotic effects of starch coated copper nanoparticles on Capan 1 pancreatic cancer cells. J. Drug. Deliv. Sci. Technol. 79 (November 2022) https://doi.org/10.1016/j.jddst.2022.104077.

Institute NC. Protocols and Capabilities from the Nanotechnology Characterization Lab. https://www.cancer.gov/nano/research/ncl/protocols-capabilities#physicochemical-characterization-protocols. Published 2023.

Irmukhametova, G.S., Mun, G.A., Khutoryanskiy, V.V., 2011. Thiolated Mucoadhesive and PEGylated Nonmucoadhesive Organosilica Nanoparticles from 3-Mercaptopropyltrimethoxysilane. Langmuir. 27 (15), 9551–9556. https://doi.org/10.1021/la201385h.

ISO 10993-5:2009(en), Biological evaluation of medical devices — Part 5: Tests for in vitro cytotoxicity. Biological evaluation of medical devices. https://www.iso.org/obp/ui/#iso:std:iso:10993:-5:ed-3:v1:en. Published 2009. Accessed April 15, 2021.

Jalali, N., Moztarzadeh, F., Mozafari, M., Asgari, S., Motevalian, M., Alhosseini, S.N., 2011. Surface modification of poly(lactide-co-glycolide) nanoparticles by d-α-tocopheryl polyethylene glycol 1000 succinate as potential carrier for the delivery of drugs to the brain. Colloids. Surfaces. A. Physicochem. Eng. Asp. 392 (1), 335–342. https://doi.org/10.1016/j.colsurfa.2011.10.012.

Kang, Z.L., Zhang, X., hua, Li X,, et al., 2021. The effects of sodium chloride on proteins aggregation, conformation and gel properties of pork myofibrillar protein Running Head: Relationship aggregation, conformation and gel properties. J. Food. Sci. Technol. 58 (6), 2258–2264. https://doi.org/10.1007/s13197-020-04736-4.

Kashif, M.ur R., Sohail, M., Khan, S.A., et al., 2022. Chitosan/guar gum-based thermoreversible hydrogels loaded with pullulan nanoparticles for enhanced nose-to-brain drug delivery. Int. J. Biol. Macromol. 215 (April), 579–595. https://doi.org/10.1016/j.ijbiomac.2022.06.161.

Khutoryanskaya, O.V., Mayeva, Z.A., Mun, G.A., Khutoryanskiy, V.V., 2008. Designing temperature-responsive biocompatible copolymers and hydrogels based on 2-hydroxyethyl(meth)acrylates. Biomacromolecules. 9 (12), 3353–3361. https://doi.org/10.1021/bm8006242.

Kim, H., Röth, D., Isoe, Y., et al., 2021. Protein corona components of polyethylene glycol-conjugated organosilica nanoparticles modulates macrophage uptake. Colloids. Surfaces. B. Biointerfaces. 199 (September 2020) https://doi.org/10.1016/j.colsurfb.2020.111527.

Krętowski, R., Kusaczuk, M., Naumowicz, M., Kotyńska, J., Szynaka, B., Cechowska-Pasko, M., 2017. The effects of silica nanoparticles on apoptosis and autophagy of glioblastoma cell lines. Nanomaterials. 7 (8) https://doi.org/10.3390/nano7080230.

Kulkarni, S.A., Feng, S.-S., 2011. Effects of surface modification on delivery efficiency of biodegradable nanoparticles across the blood-brain barrier. Nanomedicine. (Lond). 6 (2), 377–394. https://doi.org/10.2217/nnm.10.131.

Kumar, C.S.S.R., 2010. Nanotechnology tools in pharmaceutical R&D. Mater. Today. https://doi.org/10.1016/S1369-7021(10)70142-5.

Kurtz-Chalot, A., Villiers, C., Pourchez, J., et al., 2017. Impact of silica nanoparticle surface chemistry on protein corona formation and consequential interactions with biological cells. Mater. Sci. Eng. C. 75, 16–24. https://doi.org/10.1016/j.msec.2017.02.028.

Lassenberger, A., Bixner, O., Gruenewald, T., Lichtenegger, H., Zirbs, R., Reimhult, E., 2016. Evaluation of High-Yield Purification Methods on Monodisperse PEG-Grafted Iron Oxide Nanoparticles. Langmuir. 32 (17), 4259–4269. https://doi.org/10.1021/acs.langmuir.6b00919.

Lee, K.I., Su, C.C., Fang, K.M., Wu, C.C., Wu, C.T., Chen, Y.W., 2020. Ultrafine silicon dioxide nanoparticles cause lung epithelial cells apoptosis via oxidative stress-activated PI3K/Akt-mediated mitochondria- and endoplasmic reticulum stress-dependent signaling pathways. Sci. Rep. 10 (1), 1–13. https://doi.org/10.1038/s41598-020-66644-z.

Li, X., Wang, B., Zhou, S., et al., 2020. Surface chemistry governs the sub-organ transfer, clearance and toxicity of functional gold nanoparticles in the liver and kidney. J. Nanobiotechnology. 18 (1) https://doi.org/10.1186/s12951-020-00599-1.

Liu, T., Li, L., Teng, X., et al., 2011. Single and repeated dose toxicity of mesoporous hollow silica nanoparticles in intravenously exposed mice. Biomaterials. 32 (6), 1657–1668. https://doi.org/10.1016/j.biomaterials.2010.10.035.

Liu, Y.Q., Xue, S.M., Zhang, P., et al., 2020. Silica nanoparticles disturb ion channels and transmembrane potentials of cardiomyocytes and induce lethal arrhythmias in mice. Int. J. Nanomedicine. 15, 7397–7413. https://doi.org/10.2147/IJN.S261692.
Maser, E., Schulz, M., Sauer, U.G., et al., 2015. In vitro and in vivo genotoxicity investigations of differently sized amorphous SiO2 nanomaterials. Mutat. Res. Toxicol. Environ. Mutagen. 794, 57–74. https://doi.org/10.1016/J.MRGENTOX.2015.10.005.
Mendez, N., Liberman, A., Corbeil, J., et al., 2017. Assessment of in vivo systemic toxicity and biodistribution of iron-doped silica nanoshells. Nanomed. Nanotechnol.,. Biol. Med. 13 (3), 933–942. https://doi.org/10.1016/j.nano.2016.10.018.
Mishra, A., Kumar, R., Mishra, J., et al., December 2022. Strategies facilitating the permeation of nanoparticles through blood-brain barrier: An insight towards the development of brain-targeted drug delivery system. J. Drug. Deliv. Sci. Technol. 2023 (86), 104694 https://doi.org/10.1016/j.jddst.2023.104694.
Mohammadpour, R., Yazdimamaghani, M., Cheney, D.L., Jedrzkiewicz, J., Ghandehari, H., 2019. Subchronic toxicity of silica nanoparticles as a function of size and porosity. J. Control. Release. 304 (April), 216–232. https://doi.org/10.1016/j.jconrel.2019.04.041.
Mun, E.A., Morrison, P.W.J., Williams, A.C., Khutoryanskiy, V.V., 2014. On the Barrier Properties of the Cornea: A Microscopy Study of the Penetration of Fluorescently Labeled Nanoparticles. Polym.,. Sodium. Fluorescein. https://doi.org/10.1021/mp500332m.
Mun, E.A., Hannell, C., Rogers, S.E., Hole, P., Williams, A.C., Khutoryanskiy, V.V., 2014. On the Role of Specific Interactions in the Diffusion of Nanoparticles in Aqueous Polymer Solutions. Langmuir. 30 (1), 308–317. https://doi.org/10.1021/la4029035.
Mun, E.A., Williams, A.C., Khutoryanskiy, V.V., 2016. Adhesion of thiolated silica nanoparticles to urinary bladder mucosa: Effects of PEGylation, thiol content and particle size. Int. J. Pharm. 512 (1), 32–38. https://doi.org/10.1016/j.ijpharm.2016.08.026.
Murugadoss, S., Lison, D., Godderis, L., et al., 2017. Toxicology of silica nanoparticles: an update. Arch. Toxicol. 91 (9), 2967–3010. https://doi.org/10.1007/s00204-017-1993-y.
Nafee, N., Taetz, S., Schneider, M., Schaefer, U.F., Lehr, C.M., 2007. Chitosan-coated PLGA nanoparticles for DNA/RNA delivery: effect of the formulation parameters on complexation and transfection of antisense oligonucleotides. Nanomed. Nanotechnol.,. Biol. Med. 3 (3), 173–183. https://doi.org/10.1016/j.nano.2007.03.006.
Nakamura, M., Ishimura, K., 2007. Synthesis and characterization of organosilica nanoparticles prepared from 3-mercaptopropyltrimethoxysilane as the single silica source. J. Phys. Chem. C. 111 (51), 18892–18898. https://doi.org/10.1021/jp075798o.
Nakamura, M., Ishimura, K., 2008. One-pot synthesis and characterization of three kinds of thiol-organosilica nanoparticles. Langmuir. 24 (9), 5099–5108. https://doi.org/10.1021/la703395w.
Nakamura, M., Ozaki, S., Abe, M., Matsumoto, T., Ishimura, K., 2011. One-pot synthesis and characterization of dual fluorescent thiol-organosilica nanoparticles as non-photoblinking quantum dots and their applications for biological imaging. J. Mater. Chem. 21 (12), 4689–4695. https://doi.org/10.1039/c0jm04259e.
Navarro-Palomares, E., González-Saiz, P., Renero-Lecuna, C., et al., 2020. Dye-doped biodegradable nanoparticle SiO 2 coating on zinc-and iron-oxide nanoparticles to improve biocompatibility and for in vivo imaging studies †. Nanoscale 12, 6164. https://doi.org/10.1039/c9nr08743e.
Neun, B.W., Ilinskaya, A.N., Dobrovolskaia, M.A., 2018. In: Updated method for in vitro analysis of nanoparticle hemolytic properties. Humana Press Inc., pp. 91–102. https://doi.org/10.1007/978-1-4939-7352-1_9
Niu, M., Zhong, H., Shao, H., et al., 2016. Shape-Dependent Genotoxicity of Mesoporous Silica Nanoparticles and Cellular Mechanisms. J. Nanosci. Nanotechnol. 16 (3), 2313–2318. https://doi.org/10.1166/jnn.2016.10928.
Park, J.-H., Jeong, H., Hong, J., et al., 2016. The Effect of Silica Nanoparticles on Human Corneal Epithelial Cells. Sci. Rep. 6, 37762. https://doi.org/10.1038/srep37762.
Patsula, V., Horák, D., Kučka, J., et al., 2019. Synthesis and modification of uniform PEG-neridronate-modified magnetic nanoparticles determines prolonged blood circulation and biodistribution in a mouse preclinical model. Sci. Rep. 9 (1), 10765. https://doi.org/10.1038/s41598-019-47262-w.
Pelaz, B., Del Pino, P., Maffre, P., et al., 2015. Surface Functionalization of Nanoparticles with Polyethylene Glycol: Effects on Protein Adsorption and Cellular Uptake. ACS. Nano. 9 (7), 6996–7008. https://doi.org/10.1021/acsnano.5b01326.
Poon, W., Zhang, Y.N., Ouyang, B., et al., 2019. Elimination Pathways of Nanoparticles. ACS. Nano. 13 (5), 5785–5798. https://doi.org/10.1021/acsnano.9b01383.
Rascol, E., Pisani, C., Dorandeu, C., et al., 2018. Biosafety of Mesoporous Silica Nanoparticles. Biomimetics. 3 (3), 22. https://doi.org/10.3390/biomimetics3030022.
Roy, I., Ohulchanskyy, T.Y., Bharali, D.J., et al., 2005. Optical tracking of organically modified silica nanoparticles as DNA carriers: A nonviral, nanomedicine approach for gene delivery. Proc. Natl. Acad. Sci. 102 (2), 279–284. https://doi.org/10.1073/pnas.0408039101.
Schuck, R.N., Zha, W., Edin, M.L., et al. 2014. The Cytochrome P450 Epoxygenase Pathway Regulates the Hepatic Inflammatory Response in Fatty Liver Disease. Guillou H, ed. PLoS One. 9(10):e110162. https://doi.org/10.1371/journal.pone.0110162.
Shahabi, S., Treccani, L., Dringen, R., Rezwan, K., 2015. Modulation of Silica Nanoparticle Uptake into Human Osteoblast Cells by Variation of the Ratio of Amino and Sulfonate Surface Groups: Effects of Serum. ACS. Appl. Mater. Interfaces. 7 (25), 13821–13833. https://doi.org/10.1021/acsami.5b01900.
Soddu, L., Trinh, D.N., Dunne, E., et al., 2020. Identification of physicochemical properties that modulate nanoparticle aggregation in blood. Beilstein. J. Nanotechnol. 11, 550–567. https://doi.org/10.3762/bjnano.11.44.
Souris, J.S., Lee, C.H., Cheng, S.H., et al., 2010. Surface charge-mediated rapid hepatobiliary excretion of mesoporous silica nanoparticles. Biomaterials. 31 (21), 5564–5574. https://doi.org/10.1016/j.biomaterials.2010.03.048.
Sponchia, G., Marin, R., Freris, I., et al., 2014. Mesoporous silica nanoparticles with tunable pore size for tailored gold nanoparticles. J. Nanoparticle. Res. 16 (2) https://doi.org/10.1007/s11051-014-2245-1.
Sponchia, G., Marin, R., Freris, I., Marchiori, M., Moretti, E., Storaro, L., Canton, P., Lausi, A., Benedetti, A., Riello, P., 2014. Mesoporous silica nanoparticles with tunable pore size for tailored gold nanoparticles. J. Nanoparticle. Res. 16 (2) https://doi.org/10.1007/s11051-014-2245-1.
Tehrani, S.F., Bharadwaj, P., Leblond Chain, J., Roullin, V.G., 2023. Purification processes of polymeric nanoparticles: How to improve their clinical translation? J. Control. Release. 360 (July), 591–612. https://doi.org/10.1016/j.jconrel.2023.06.038.
Tsai, P.H., Wang, M.L., Chang, J.H., et al., 2019. Dual Delivery of HNF4α and Cisplatin by Mesoporous Silica Nanoparticles Inhibits Cancer Pluripotency and Tumorigenicity in Hepatoma-Derived CD133-Expressing Stem Cells. ACS. Appl. Mater. Interfaces. 11 (22), 19808–19818. https://doi.org/10.1021/acsami.9b04474.
Urata, C., Aoyama, Y., Tonegawa, A., Yamauchi, Y., Kuroda, K., 2009. Dialysis process for the removal of surfactants to form colloidal mesoporous silica nanoparticles. Chem. Commun. 34, 5094–5096. https://doi.org/10.1039/b908625k.
Villanueva-Flores, F., Castro-Lugo, A., Ramírez, O.T., Palomares, L.A., 2020. Understanding cellular interactions with nanomaterials: Towards a rational design of medical nanodevices. Nanotechnology. 31 (13) https://doi.org/10.1088/1361-6528/ab5bc8.
Wang, X., Meng, X., Mao, K., et al., December 2022. Maleimide as the PEG end-group promotes macrophage-targeted drug delivery of PEGylated nanoparticles in vivo by enhancing interaction with circulating erythrocytes. Biomaterials. 2023 (300), 122187 https://doi.org/10.1016/j.biomaterials.2023.122187.
Wang, D.-P., Wang, Z.-J., Zhao, R., et al., 2020. Silica nanomaterials induce organ injuries by Ca 2+-ROS-initiated disruption of the endothelial barrier and triggering intravascular coagulation. Part. Fibre. Toxicol. 17 (1) https://doi.org/10.1186/s12989-020-00340-8.
Ways, T.M.M., Lau, W.M., Ng, K.W., Khutoryanskiy, V.V., 2018. Synthesis of thiolated, PEGylated and POZylated silica nanoparticles and evaluation of their retention on rat intestinal mucosa in vitro. Eur. J. Pharm. Sci. 122 (June), 230–238. https://doi.org/10.1016/j.ejps.2018.06.032.
Ways, T.M.M., Ng, K.W., Lau, W.M., Khutoryanskiy, V.V., 2020. Silica nanoparticles in transmucosal drug delivery. Pharmaceutics. 12 (8), 1–25. https://doi.org/10.3390/pharmaceutics12080751.
Wozniak, M.J., Wozniak, P., Bystrzejewski, M., et al., 2006. Magnetic nanoparticles of Fe and Nd-Fe-B alloy encapsulated in carbon shells for drug delivery systems: Study of the structure and interaction with the living cells. J. Alloys. Compd. 423 (1–2 SPEC. ISS.), 87–91. https://doi.org/10.1016/j.jallcom.2005.12.028.
Xiong, L., Qiao, S.Z., 2016. A mesoporous organosilica nano-bowl with high DNA loading capacity-a potential gene delivery carrier. Nanoscale. 8 (40), 17446–17450. https://doi.org/10.1039/c6nr06777h.
Yan, J., Ji, S., Chang, T., et al., November 2022. Construction of bionic nanoparticles camouflaged with macrophage membranes for drug delivery in breast cancer. J. Drug. Deliv. Sci. Technol. 2023 (84), 104433 https://doi.org/10.1016/j.jddst.2023.104433.
Yang, B., Chen, Y., Shi, J., 2019. Mesoporous silica/organosilica nanoparticles: Synthesis, biological effect and biomedical application. Mater. Sci. Eng. R. Reports. 137 (January), 66–105. https://doi.org/10.1016/j.mser.2019.01.001.
Yim, B., Park, J.H., Jeong, H., et al., 2017. The effects of nonporous silica nanoparticles on cultured human keratocytes. Investig. Ophthalmol. Vis. Sci. 58 (1), 362–371. https://doi.org/10.1167/iovs.16-20603.
Yu, T., Hubbard, D., Ray, A., Ghandehari, H., 2012. In vivo biodistribution and pharmacokinetics of silica nanoparticles as a function of geometry, porosity and surface characteristics. J. Control. Release. 163 (1), 46–54. https://doi.org/10.1016/j.jconrel.2012.05.046.
Yu, L., Lin, H., Lu, X., Chen, Y., 2018. Multifunctional Mesoporous Silica Nanoprobes: Material Chemistry-Based Fabrication and Bio-Imaging Functionality. Adv. Ther. 1 (8), 1800078. https://doi.org/10.1002/adtp.201800078.
Zhang, J., Rana, S., Srivastava, R.S., Misra, R.D.K., 2008. On the chemical synthesis and drug delivery response of folate receptor-activated, polyethylene glycol-functionalized magnetite nanoparticles. Acta. Biomater. 4 (1), 40–48. https://doi.org/10.1016/j.actbio.2007.06.006.
Zhou, F., Liao, F., Chen, L., Liu, Y., Wang, W., Feng, S., 2019. The size-dependent genotoxicity and oxidative stress of silica nanoparticles on endothelial cells. Environ. Sci. Pollut. Res. 26 (2), 1911–1920. https://doi.org/10.1007/s11356-018-3695-2.
Zhou, F., Li, H., Liu, Y., Deng, H., Rong, J., Zhao, J., November 2022. Hyaluronan derivative decorated calcium carbonate nanoparticle as a potential platform for breast cancer synergistic therapy via blood coagulation and drug delivery. J. Drug. Deliv. Sci. Technol. 2023 (83), 104406 https://doi.org/10.1016/j.jddst.2023.104406.